frontiers in Ecology and Evolution

ORIGINAL RESEARCH
published: 10 August 2021
doi: 10.3389/fevo.2021.709766

Braincase and Inner Ear Anatomy of the Late Carboniferous Tetrapod *Limnoscelis dynatis* (Diadectomorpha) Revealed by High-Resolution X-ray Microcomputed Tomography

Jozef Klembara[1], Marcello Ruta[2], Miroslav Hain[3] and David S. Berman[4]*

[1] Department of Ecology, Faculty of Natural Sciences, Comenius University in Bratislava, Bratislava, Slovakia, [2] Joseph Banks Laboratories, School of Life Sciences, University of Lincoln, Lincoln, United Kingdom, [3] Institute of Measurement Science, Slovak Academy of Sciences, Bratislava, Slovakia, [4] Carnegie Museum of Natural History, Section of Vertebrate Paleontology, Pittsburgh, PA, United States

OPEN ACCESS

Edited by:
Mark Joseph MacDougall, Museum of Natural History Berlin (MfN), Germany

Reviewed by:
Jun Liu, Institute of Vertebrate Paleontology and Paleoanthropology, Chinese Academy of Sciences, China
Julien Benoit, University of the Witwatersrand, South Africa

***Correspondence:**
Jozef Klembara
jozef.klembara@uniba.sk

Specialty section:
This article was submitted to Paleontology, a section of the journal Frontiers in Ecology and Evolution

Received: *14 May 2021*
Accepted: *01 July 2021*
Published: *10 August 2021*

Citation:
Klembara J, Ruta M, Hain M and Berman DS (2021) Braincase and Inner Ear Anatomy of the Late Carboniferous Tetrapod Limnoscelis dynatis (Diadectomorpha) Revealed by High-Resolution X-ray Microcomputed Tomography. Front. Ecol. Evol. 9:709766. doi: 10.3389/fevo.2021.709766

The braincase anatomy of the Pennsylvanian diadectomorph *Limnoscelis dynatis* is described in detail, based upon high-resolution X-ray microcomputed tomography. Both supraoccipitals and most of the prootics and opisthotics are preserved. The known portions of the left prootic, opisthotic, and supraoccipital enclose complete sections of the endosseous labyrinth, including the anterior, posterior, and lateral semicircular canals, the vestibule, the cochlear recess, and the canal for the endolymphatic duct. The fossa subarcuata is visible anteromedial to the anterior semicircular canal. The presumed endolymphatic fossae occur in the dorsal wall of the posteromedial portion of the supraoccipital. Both the fossa subarcuata and the fossa endolymphatica lie in the cerebellar portion of the cranial cavity. In order to investigate the phylogenetic position of *L. dynatis* we used a recently published data matrix, including characters of the braincase, and subjected it to maximum parsimony analyses under a variety of character weighting schemes and to a Bayesian analysis. *Limnoscelis dynatis* emerges as sister taxon to *L. paludis*, and both species form the sister group to remaining diadectomorphs. Synapsids and diadectomorphs are resolved as sister clades in ∼90% of all the most parsimonious trees from the unweighted analysis, in the single trees from both the reweighted and the implied weights analyses, as well in the Bayesian tree.

Keywords: Diadectomorpha, computed tomography, endocranial anatomy, inner ear, phylogeny

INTRODUCTION

The origin and diversification of amniotes are at the center of considerable resurgent interest motivated by novel phylogenetic hypotheses (e.g., Ford and Benson, 2019, 2020), new evidence from reproductive paleoecology (e.g., Maddin et al., 2020) and key findings in comparative anatomy, developmental biology, and paleontology (e.g., Kuratani et al., 2011; Schoch and Sues, 2019). Crown-group amniotes are estimated to have originated some 320 million years

ago (Jones et al., 2018; Klembara et al., 2020a,b, and references therein; see also estimates in www.timetree.org). They are diagnosed by several anatomical and, in the case of extant taxa, physiological traits, notably those pertaining to reproduction.

For over a century one particular clade of early tetrapods, the diadectomorphs, has played a pivotal role in debates about amniote ancestry. Diadectomorphs are known from the Kasimovian-Gzhelian of Euramerica and the Wuchiapingian of China (see Liu and Bever, 2015). Traditionally placed as the immediate sister taxon to crown-group amniotes, they have occasionally been allied to synapsids (e.g., Case, 1907, 1914), a hypothesis of relationship that has received formal cladistic support (see Berman, 2000, 2013; Klembara et al., 2020b). Our knowledge of diadectomorph anatomy has recently been enriched by a wealth of new neuroanatomical data. Thus, Klembara et al. (2020a,b) provided a detailed description of the braincase and inner ear of the diadectomorphs *Diadectes absitus* and *Orobates pabsti* using high-resolution X-ray microcomputed tomography. The well-developed inner ear of both species displays a similar overall morphology to that of several extant and extinct amniotes, e.g., in the possession of a distinct and pyramid-like cochlear recess. Unlike extant amniotes, in which the cochlear recess occurs ventral to the vestibule, the recess in *D. absitus* and *O. pabsti* lies posterior to the vestibule, a condition also observed in the stem-group amniote *Seymouria baylorensis* (Klembara et al., 2020b). This anatomical construction is in striking contrast to that of extant amphibians, in which the cochlear recess is not developed, and the sensory hair cells associated with hearing are situated in the posterior portion of the vestibule (lagenar macula). These observations led Klembara et al. (2020b) to conclude that the inner ears of *D. absitus* and *O. pabsti* display a combination of plesiomorphic (e.g., position of the cochlear recess) and apomorphic features (e.g., presence and morphology of the recess and its size relative to the vestibule), some of which appear to be morphologically transitional between those of amniotes and non-amniote tetrapods.

Diadectomorphs are mostly known from adult specimens (e.g., Olson, 1947; Berman et al., 1992, 1998, 2010; Berman, 2013; Klembara et al., 2020a). In these instances, the bones enclosing the endosseous labyrinth—supraoccipital, prootic and opisthotic—fuse in varying degrees, so that detailed neuroanatomical observations are difficult (Klembara et al., 2020a). Immature specimens are rare (e.g., *Diadectes sanmiguelensis* Lewis and Vaughn, 1965 and smallest specimens of *Orobates pabsti* Berman et al., 2004). In addition, only two subadult specimens have been investigated thus far using advanced CT-scanning and image analysis techniques, namely *Diadectes absitus* specimen MNG 8747 and *Orobates pabsti* specimen MNG 10181, both with skull lengths of about 12.5 cm (Klembara et al., 2020a,b).

In this paper we significantly add to the existing knowledge of the neurocranial and inner ear anatomy of diadectomorphs by providing a detailed description of a partial braincase belonging to the Late Pennsylvanian *Limnoscelis dynatis* Berman and Sumida, 1990. The specimen in question is of considerable importance because its left supraoccipital, prootic and opisthotic are almost fully articulated and enclose a nearly complete endosseous labyrinth. The aims of this paper are to describe the endocranial bones and endosseous labyrinth of *L. dynatis*, to reconstruct its inner ear using virtual 3D models of its constituent bones and to carry out a cladistic analysis of amniote-like tetrapods based upon a revised version of the data matrix in Klembara et al. (2020b), whose anatomical terminology we follow.

Institutional Abbreviations

CM, Carnegie Museum of Natural History, Pittsburgh, United States; MNG, Museum der Natur, Gotha, Germany; YPM, Yale Peabody Museum, New Haven, United States.

MATERIALS AND METHODS

Age, Locality, and General Remarks on Preservation

The incomplete braincase of specimen CM 47653 (**Figures 1–13**), described by Berman and Sumida (1990) as part of the holotype of *Limnoscelis dynatis*, originates from the late Pennsylvanian black shales of the Sangre de Cristo Formation in central Colorado, United States. The posterior portion of the braincase encloses the endosseous labyrinth of the inner ear. As shown in **Figure 1**, the braincase consists of the lateral halves of the bipartite supraoccipital, most of the posterior half of the left prootic, the right prootic lacking its anterior portion, and the incomplete halves of the opisthotics. The left supraoccipital, prootic and opisthotic are preserved in anatomical articulation, whereas their right counterparts are disarticulated. The external surfaces of the three elements consist of a thin layer of dense compact bone. In contrast, their internal surfaces consist mostly of cancellous bone (**Figures 2A,B, 3–5, 10, 11**). The supraoccipitals are nearly complete with the right slightly overlapping the left. Berman and Sumida (1990) considered the two supraoccipitals to be portions of an unpaired, anteroposteriorly broken bone. Following additional preparation and restudy of the specimen, Berman (2000) realized that the supraoccipital is paired. Our investigations confirm Berman's interpretation. The medial margin of the left supraoccipital is strongly disrupted due to incomplete preservation, whereas the medial margin of the right supraoccipital is well-preserved along a short and smooth posterior portion of its course. This surface consists of compact bone, and its texture resembles that of the other three braincase elements (**Figures 2C,D**). This observation allows us to conclude that in this specimen the supraoccipitals are represented by paired independent ossifications. Therefore, we infer that this specimen may represent a juvenile. Only an incomplete section of the posterior region of the left prootic is preserved. The right prootic is more complete than its left antimere. It contacts the medial portion of the ventral surface of the supraoccipital and the lateral portion of the opisthotic (**Figures 1, 3**). Its internal surface can only be accessed in the scans. Both the paroccipital process and posteromedial portion of the left opisthotic are missing. The better preserved right opisthotic shows most of the paroccipital process and the entire posteromedial portion of its corpus, the latter including the otic

through (Berman and Sumida, 1990; **Figures 1A,B**). Due to dorsoventral compression the posteromedial portion of the right opisthotic shows an exaggerated posterior inclination. In life, this portion would be nearly vertically orientated (Fracasso, 1987; Berman et al., 2010; see also below). The internal structures of the right opisthotic are damaged, and it is therefore impossible to segment the portion of the endosseous labyrinth enclosed within it. In contrast, the endosseous labyrinth appears well preserved within the left supraoccipital, prootic, and opisthotic. The broken and ventrally displaced ventral portion of the left opisthotic can be recognized on the slightly disrupted rounded surface that forms the dorsolateral wall of the vestibule (**Figure 2A**). This allowed us to reconstruct the portion of the vestibule that is adjacent to the wall (**Figure 2B**). We were also able to segment the cavities of the endosseous labyrinth and to assemble a virtual 3D model of the latter.

Microcomputed Tomography Imaging

To obtain high-resolution microCT scans, we used the Nanotom 180 X-ray microtomography system (GE Phoenix), fitting the X-ray tube with a tungsten target in micro-focusing mode M0. For outgoing X-ray radiation, beam filtering was attained with a 0.2 mm thick Cu plate. The accelerating voltage was set to 160 kV with beam current of 90 μA. The detector timing was 750 ms. No pixel binning was used, and the voxel size was 27 μm. Through the duration of the scanned object's rotation, 1,800 two-dimensional X-ray projections were recorded. For 3D volume reconstruction, we used the datos| x CT software (GE Phoenix). The 3D volume data sets were filtered, rendered, and segmented in VGStudio MAX 2.1 (Volume Graphics). For the volume data rendering (2D projection of 3D volume data), we applied the isosurface and volume rendering algorithms. For the segmentation of volume data, the region growing method was largely employed, along with the opening/closing and the erosion/dilation image processing techniques. The final smoothing of the 3D model surfaces of segmented objects was achieved with the open-source program MeshLab v2020.7.

Phylogenetic Analysis

We investigated the interrelationships of *Limnoscelis dynatis* by coding relevant information from its cranial and postcranial skeleton into the data matrix used by Klembara et al. (2020b). Cranial and postcranial characters were scored in light of Berman and Sumida's (1990) work, whereas neurocranial characters were scored in light of the new data provided here. The matrix consisted of 55 taxa and 294 characters (278 parsimony-informative). We added two cranial and four postcranial characters to the character list in Klembara et al. (2020b; new characters are appended to the end of the list). The list of taxa was left unaltered except for the inclusion of *L. dynatis*. The data matrix was processed under maximum parsimony and Bayesian inference. The data matrix in PAUP-ready Nexus format and the list of characters are in **Supplementary Material (Data Sheets 1 and 2)**.

For the parsimony analyses, we applied three character weighting criteria: (1) equally weighted characters; (2) characters reweighted by the maximum value of their rescaled consistency index obtained from the equally weighted analysis; and (3) implied weights with a constant of concavity value of 6 (Goloboff, 1993). All parsimony analyses were carried out in PAUP* (Swofford, 1998; v. 4.0a build 169). Searches for the most parsimonious trees were conducted using heuristic methods, applying the tree bisection-reconnection branch-swapping algorithm with 10,000 random stepwise taxon addition sequences, and holding one tree in memory at each replicate. Subsequently, we applied 10 rounds of the same algorithm to trees stored in memory from the initial search, but enforcing the multiple trees saving option. Node support was evaluated by applying bootstrap (Felsenstein, 1985) and jackknife (Farris et al., 1996) resampling methods, using 10,000 random character resampling replicates under the fast stepwise addition option. In order to establish whether the data matrix includes phylogenetic information, we compared the ensemble consistency index value of the trees obtained from the unweighted parsimony analysis with theoretical threshold values, that are expected for matrices of comparable taxon numbers, following protocols in Sanderson and Donoghue (1989) and Klassen et al. (1991).

For the Bayesian analysis, we employed MrBayes (Ronquist and Huelsenbeck, 2003; v. 3.2.6) under the standard model for morphological data and gamma-distributed rate changes across characters. We ran four chains for $2{\cdot}10^7$ generations, discarding 25% of the obtained samples. The results were summarized as a 50% majority-rule consensus of resulting posterior probability tree topologies with appended credibility values. Convergence was evaluated with the Gelman and Rubin's (1992) Potential Scale Reduction Factor.

RESULTS

Braincase and Endosseous Labyrinth

As the constituent elements of the partial braincase of CM 47653 were described in detail by Berman and Sumida (1990), our contribution focuses solely on the new anatomical features obtained through high resolution X-ray microcomputed tomography, particularly those of the endosseous labyrinth and inner ear (see **Supplementary Material Data Sheet 3**).

Together, the two supraoccipitals form a plate-like element that is longer than wide and with the lateral margins orientated slightly dorsolaterally (**Figure 1**). A narrow triangular embayment occurs between the posteromedian margins of the supraoccipitals, with its apex pointing almost directly anteriorly. The surfaces of these margins are smooth (**Figure 3A**), and thus similar in texture to the short section of the medial margin of the right supraoccipital (**Figures 2C,D**). On either side of the embayment the occipital surface of the supraoccipital is occupied by a roughly semielliptical shallow area characterized by a distinct rugose surface (**Figure 1D**). This area is delimited by a shallow groove surrounded by a distinct wall. Further laterally, this area continues smoothly into a similarly shaped area visible on the occipital surface of the opisthotic (**Figure 1D**). The two areas form the articulation surface for the exoccipital (see below).

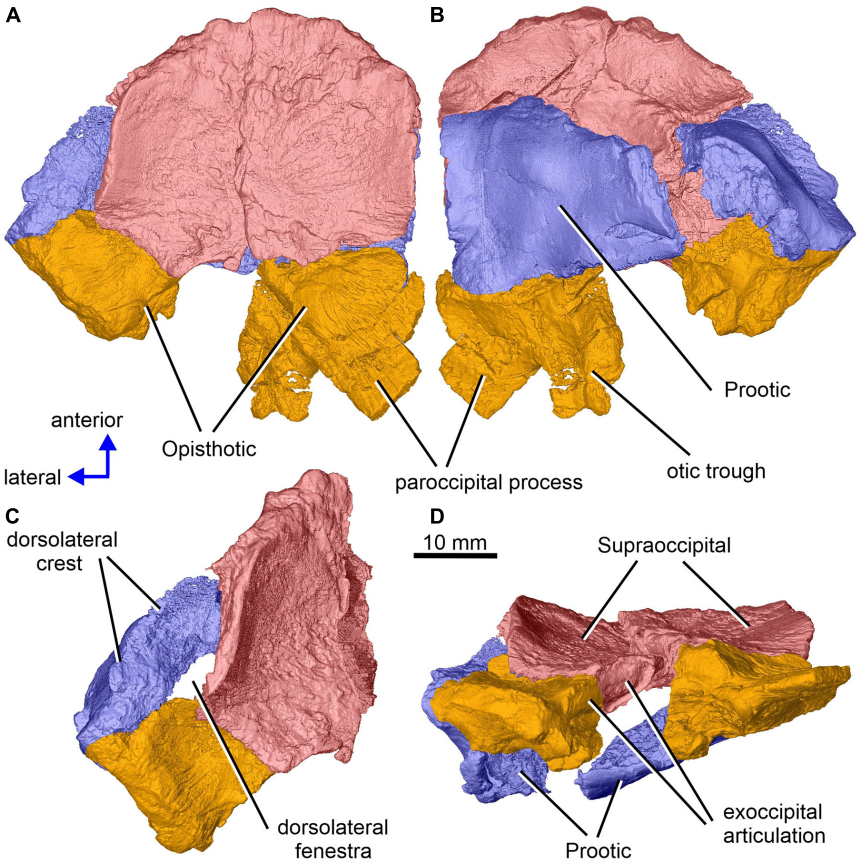

FIGURE 1 | *Limnoscelis dynatis*, CM 47653. Partial braincase in dorsal **(A)**, ventral **(B)**, dorsolateral **(C)** and posterior **(D)** views.

The dominant feature on the ventral surface of each supraoccipital half is a ventral crest, the posterior section of which medially separates the cranial cavity from the lateral cavity of the inner ear (**Figure 3**). The posterior sections of the two supraoccipital ventral crests run anterolaterally to posteromedially. At about the mid-length of the supraoccipital, each ventral crest changes its course, such that its anterior section runs anteromedially. In the anterior portions of the supraoccipitals the two crests approach one another, but preservation makes it difficult to ascertain whether they met mid-sagittally. The anterior sections of the two crests mark the posteromedial boundaries of large, paired, sub-elliptical excavations situated anterolaterally. These excavations are bordered posteriorly by a tall, robust ridge that extends nearly transversely and is characterized by a slight, anteriorly concave curvature. The smooth surface of the two anterolateral excavations presumably housed the optic lobe (or tectum opticum) in life. The large median excavation delimited by the posterior sections of the two ventral crests accommodated the cerebellum (**Figure 3**).

A distinct shallow excavation is visible on the ventral surface of the supraoccipital. It occurs posteromedial to the point where the anterior and posterior sections of each of the two ventral ridges converge, and anteromedial to the anterior semicircular canal. This excavation is likely to correspond to the fossa subarcuata (**Figures 3B,C**, **4A,D**; see Klembara et al., 2020b), an excavation that houses a small process of the dura mater as well as the cerebellar flocculus (auricule) in both extant and extinct amniotes (see below).

The sections of both the anterior and posterior semicircular canals are well preserved in both supraoccipitals (**Figures 4**, **5**). The medial section of the anterior semicircular canal opens on the ventrolateral surface of the ventral crest, and its course can be followed within the prootic (**Figures 4B,D**, **8C**). The medial section of the posterior semicircular canal opens on the ventral portion of the posterolateral edge of the supraoccipital and continues into the opisthotic (**Figures 3C**, **7C**). The crus commune opens on the ventral wall of the ventral crest (**Figure 5**). A short, medially directed canal for the endolymphatic duct (**Figures 3C**, **4B,D**) is visible close to the ventral crest. A hemi-spherical excavation occupies the posteroventral wall of both halves of the supraoccipital, which lie medial to the ventral crest and immediately lateral to the midsagittal plane. This excavation may correspond to the fossa endolymphatica, which accommodated the endolymphatic sac in life (**Figures 3B,C**, **4C,D**). The right fossa is only partially preserved due to damage caused by compression against

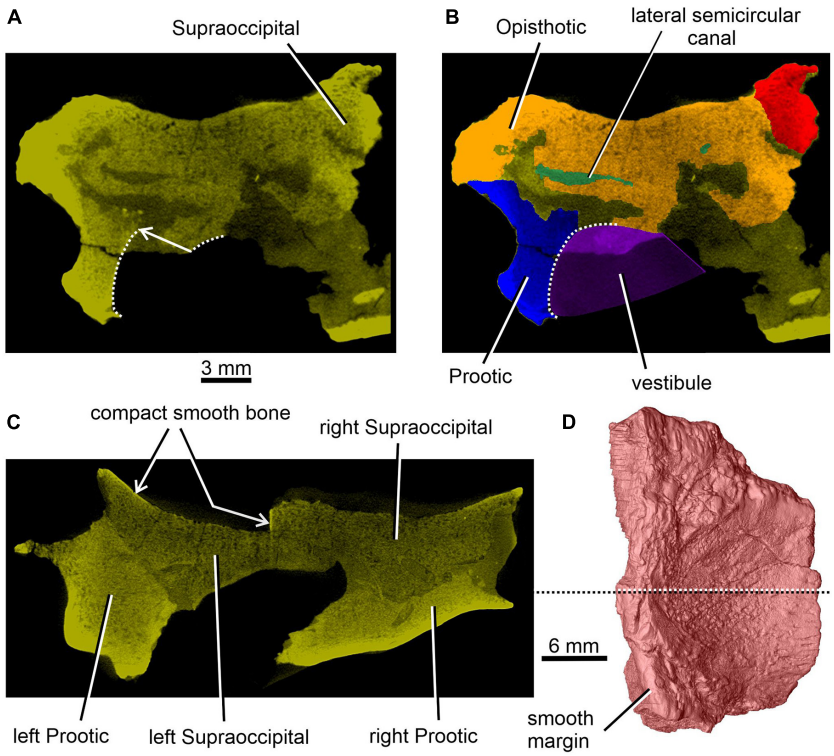

FIGURE 2 | *Limnoscelis dynatis*, CM 47653. **(A,B)** Transverse CT section through the posterior portion of the lateral semicircular canal. **(C)** Transverse CT section through the braincase at about mid-length of the right supraoccipital **(D)**.

the underlying left supraoccipital. The preserved portion of the canal for the endolymphatic duct occurs anterolateral to it (**Figures 3B,C**, **4D**).

The left paroccipital process is missing, but a large portion of the right process can be seen on the right opisthotic (**Figures 1**, **6**). The sculptured dorsal wall of the opisthotic forms a shallow depression. Two facets for the exoccipital articulation are present on the posterior surface of the posteromedial portion of the right opisthotic (**Figures 6A,B**). Between the two facets is a groove, which Berman and Sumida (1990) interpreted as a jugular groove (**Figures 6A,B**). A concavity on the internal surface of the posteromedial portion of the right opisthotic, which would be orientated ventrolaterally in life, represents the otic trough (Berman and Sumida, 1990; **Figures 6C–E**). Its distal part forms the posterior margin of the fenestra vestibuli (Berman and Sumida, 1990; **Figure 6**). The trough widens gradually anterodorsally toward the posterior wall of the vestibule (**Figures 6C–E**). Anterolateral to the trough the opisthotic displays a robust, arch-like, mediolaterally orientated ridge that participates in the formation of the posterodorsal margin of the otic capsule (**Figures 6C–E**). A similar ridge in direct continuation with the opisthotic ridge is present on the posterior portion of the prootic (**Figure 10A**). The junction of the dorsal portions of these ridges is visible on the left side of the braincase.

Enclosed within the posteromedial portion of the left opisthotic is a complete cochlear recess. In its posteriormost portion the recess is round, whereas further anteriorly it deepens gradually in a dorsoventral direction (**Figure 7A**) before merging smoothly into the vestibule (**Figures 5**, **7B**). The posterior sections of the lateral and posterior semicircular canals project from the dorsal part of the posteriormost portion of the vestibule (**Figure 7B**), with the root section of the former being about four times as long as the root section of the latter (**Figures 12**, **13D,F**). After a short tract the lateral semicircular canal first widens anteroposteriorly and then narrows again as it approaches the prootic (**Figures 5**, **13D**). The lateral section of the lateral semicircular canal is enclosed by the opisthotic (**Figures 5**, **7C**), but most of its course is encased within the prootic (**Figures 8B**, **12**). The posterior semicircular canal runs anteromedially through the opisthotic and continues anteriorly within the supraoccipital (**Figures 7B,C**). The absence of swollen regions in the prootic and opisthotic suggests that ampullae are absent (but see also discussion in Klembara et al., 2020b).

Most of the posterior region of the left prootic is preserved, although its posteriormost and ventralmost portions are missing (**Figures 1**, **3B,C**, **8A,B**). The preserved portion has a robust construction. It is mediolaterally broad and contains most of the anteroposterior tract of the lateral semicircular canal (**Figures 8B**, **12A**). Posteromedially it is sutured with the opisthotic (**Figures 1A,C**, **3B,C**, **5**, **7C**, **8D,E**). A thin, sharp crest, the crista dorsolateralis, extends slightly dorsally and distinctly laterally from the dorsal wall of this part of the prootic (**Figures 1A,C**, **8A–C**). The prootic has a smooth lateral wall

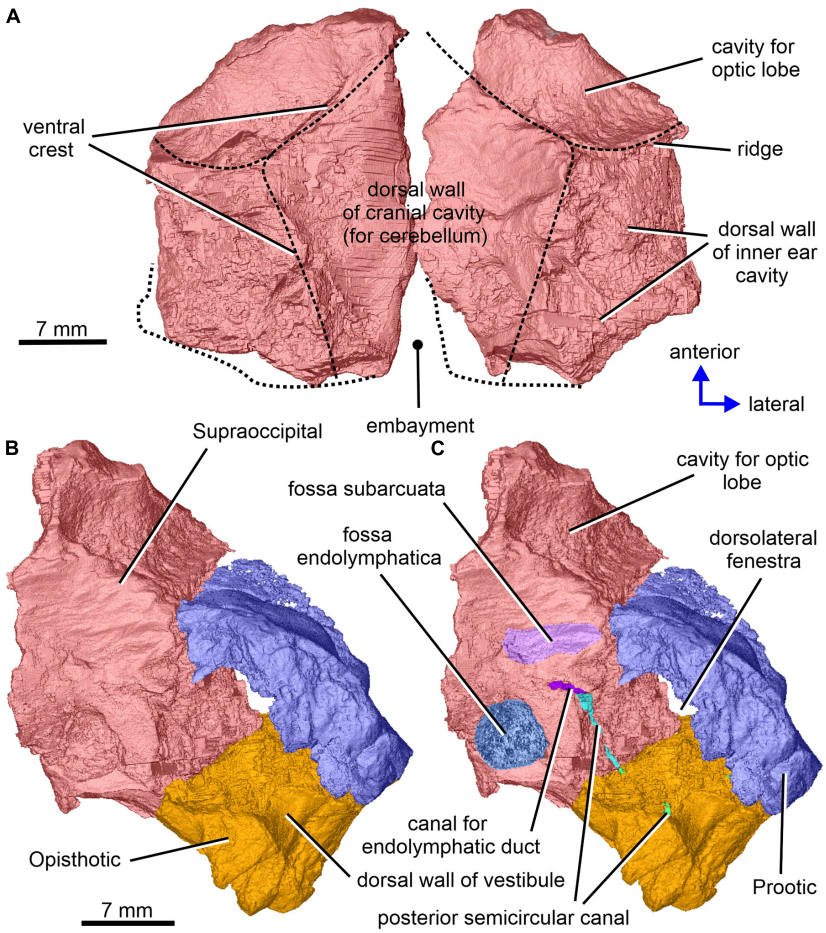

FIGURE 3 | *Limnoscelis dynatis*, CM 47653. **(A)** Supraoccipitals in ventral view. **(B,C)** Articulated left supraoccipital, prootic and opisthotic in ventromedial view.

that extends laterally into a parotic crest, the latter indicating the course of the lateral semicircular canal (**Figures 8A,B**). The latter canal is mostly enclosed within bone in the posterior portion of the anteroposterior extension of the prootic. More anteriorly the medial part of the lateral semicircular canal is partially exposed and communicates with the vestibule (**Figures 4B,C**, **8D,E**). Immediately ventromedial to the canal the excavated medial surface of the prootic delimits the smooth lateral wall of the vestibule (**Figures 8D,E**).

The right prootic is well preserved, although the anterior portion is missing (**Figures 1B**, **9–11**), and the sharp, dorsalmost portion of its dorsolateral crest is broken (**Figure 9A**). The smooth lateral wall of the right prootic is occupied by an anteroposteriorly elongate fossa in the anteroventral part of the bone (**Figure 9A**). According to Berman and Sumida (1990, figure 4B), this fossa is associated with the facial nerve. A narrow groove running anteriorly from the anterior portion of the fossa opens on the anterior margin of the preserved part of the prootic (**Figure 9A**). A canal running mediodorsally from the dorsal portion of the fossa opens on the medial wall of the prootic (**Figures 9B**, **10A,C**). Lastly, a narrow canal enclosed in bone runs posteroventrally from the posterior portion of the fossa and opens on the ventrolateral wall of the prootic as a short groove (**Figure 9A**). In life, the facial nerve probably entered the medial wall of the prootic (**Figure 10C**) and continued ventrolaterally within the bone (**Figure 9B**). The fossa may have housed the ganglion of the facial nerve (**Figure 9B**). From this point the palatal ramus of this nerve would run anteriorly along the narrow groove on the lateral wall of the prootic, whereas the hyomandibular ramus would run posteroventrally along a canal within the prootic (**Figures 9**, **10A,C**).

The posterior end of the right prootic shows a distinct crest (**Figures 9A,B**, **10**). The internal surface of the prootic is mostly cancellous, but the walls of the inner ear structures are mostly smooth (**Figures 10A,C**). The canal for the entrance of the facial nerve is anterior to the anterior section of the lateral semicircular canal (**Figures 10A,B**). The prootic is tallest in its well-preserved posterior portion. Its anteriorly excavated posteromedial wall is delimited by a sharp medial ridge running dorsoventrally (**Figure 10**). Based upon the condition of its left counterpart, it is concluded that the ridge, although partially damaged, abutted against a corresponding ridge present on the opisthotic, thereby sealing off the otic cavity posteriorly. A distinct lateral excavation occupies the posteroventral portion of the prootic,

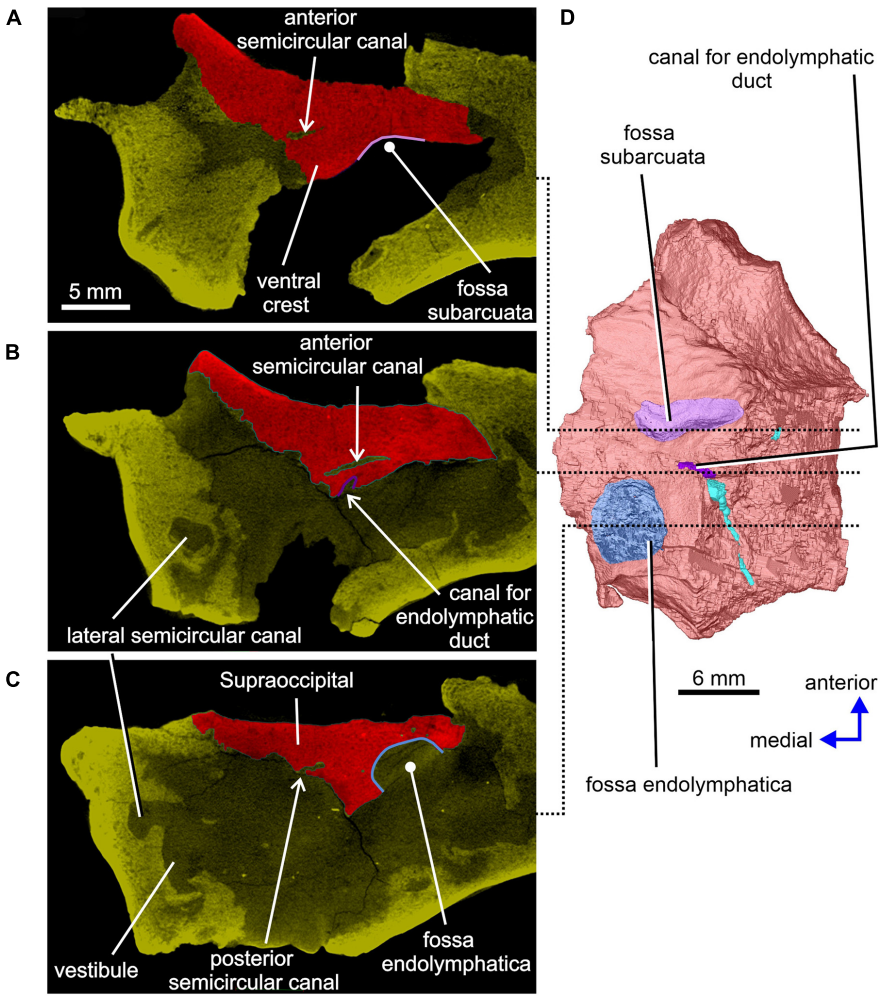

FIGURE 4 | *Limnoscelis dynatis*, CM 47653. **(A–C)** Transverse CT sections through the supraoccipital in anterior to posterior sequence. **(D)** Left supraoccipital in ventral view.

thus forming the internal wall of the fenestra vestibuli (Berman and Sumida, 1990; **Figures 9**, **10**). In life the posteromedial portion of the opisthotic would be orientated ventrolaterally, thus forming the posterior wall of the fenestra vestibuli (**Figure 6**), which faces ventrally and slightly posteriorly. A deep smooth groove emerging from the internal margin of the fenestra vestibuli runs anterodorsally along the medial wall of the prootic (**Figures 10A,B**, **11**). The groove is likely to correspond to the otic tube, and its course can be traced between the anterior and posterior portions of the vestibule (**Figures 10A,C**, **11**). Ventrally, the groove is broad and delimited by distinct, tall margins (**Figures 10A,C**). Further anterodorsally, the groove becomes gradually shallower, and its dorsal end opens into the middle portion of the vestibule (**Figures 10A,C**, **11**). The well-preserved, circular anterior portion of the vestibule (**Figures 10A,C, 11A,B**) has a smooth surface and distinct margins.

An anteroposteriorly elongate space delimited by the posterolateral margin of the supraoccipital, the posterodorsal margin of the prootic and the abbreviated anterodorsal margin of the opisthotic corresponds to a dorsolateral fenestra (**Figures 1A,C**).

Inner Ear

Figure 12A shows the position of the virtual 3D model of the inner ear within the braincase. The inner ear consists of the vestibule, the three semicircular canals, cochlear recess, and canal for the endolymphatic duct (**Figures 12**, **13**). There is no evidence of ampullae (see above). The anteroposteriorly elongate vestibule is larger and deeper in its posterior portion than in its anterior portion. The dorsal wall of the posterior portion has a slightly convex surface. In contrast, the anterior wall of the vestibule is distinctly concave. Posteriorly, the vestibule merges indistinctly into the cochlear recess (**Figures 12**, **13B–F**). The approximate boundary between the two structures is believed to coincide with the region where the posterior extremities of the posterior and the lateral semicircular canals enter the vestibule (**Figures 7B**, **12**, **13B**).

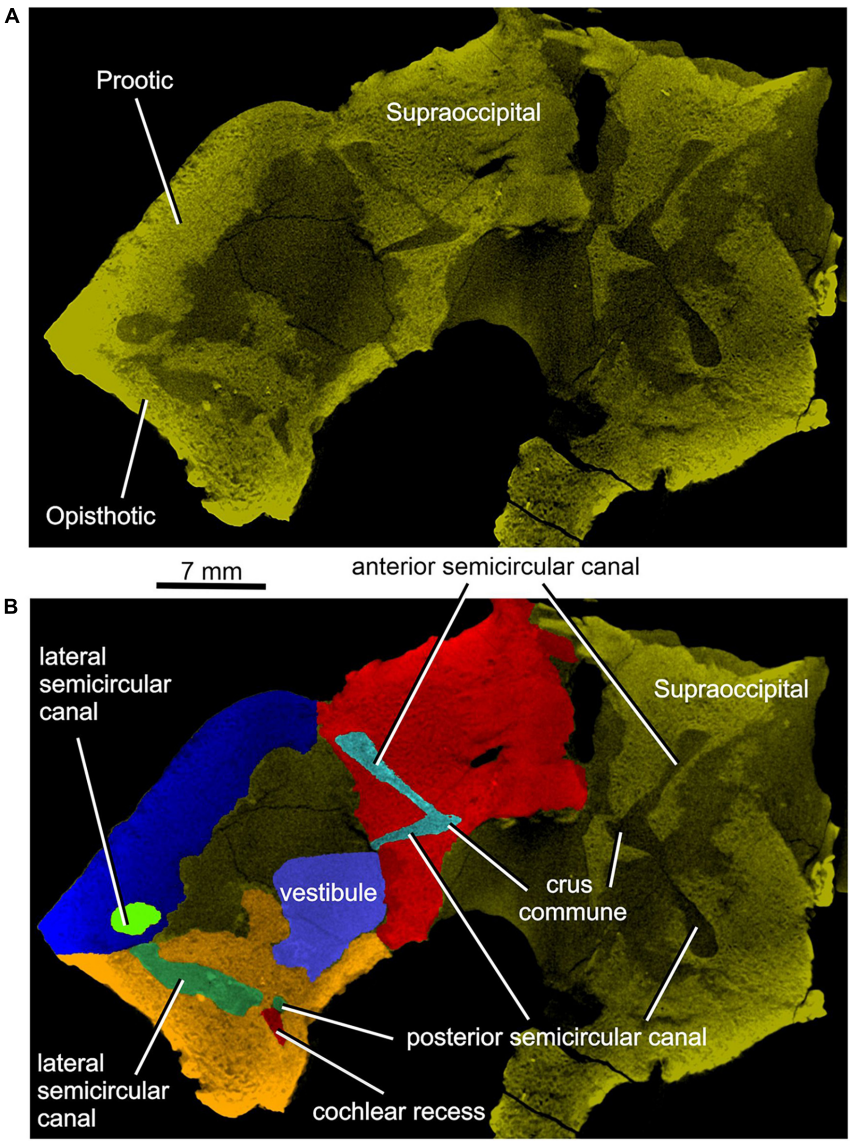

FIGURE 5 | *Limnoscelis dynatis*, CM 47653. **(A,B)** Longitudinal CT sections through the anterior and posterior semicircular canals.

The arcuate anterior semicircular canal occurs within the supraoccipital and prootic (**Figures 5**, **12**, **13**). Its medial section within the supraoccipital is widest where it contacts the crus commune. From this point the canal narrows gradually anteroposteriorly to a point situated approximately at its mid-length. Beyond this point the canal first widens and then narrows again before entering the prootic (**Figure 8C**). The lateral portion of the anterior semicircular canal exhibits a ventrolateral orientation and merges abruptly into the much thicker lateral semicircular canal (**Figures 12**, **13A–D**). The absence of ampullae and the abrupt transition from a thin anterior canal to a thick lateral canal presumably marks the border between the anterior and lateral semicircular canals (**Figures 12**, **13A,C–F**).

The lateral semicircular canal is accommodated within the prootic and opisthotic, and its morphology differs remarkably in these two bones (**Figures 12**, **13D,F**). The prootic section of the lateral semicircular canal is the most robust of all sections in all three semicircular canals and is only slightly curved anteriorly. At about the middle one-third of its course, the medial wall of the canal opens into the otic cavity immediately above the vestibule (**Figures 8D,E**). Further anteriorly this wall communicates with the vestibule (**Figures 4C**, **13F**). The posteriormost part of the prootic section of the lateral semicircular canal thins gradually and continues into the opisthotic. Within the opisthotic, the canal is narrower and turns abruptly medially (**Figure 13D**). After a short course, it widens rapidly and becomes dorsoventrally flat (**Figures 12**, **13**). At the point where it passes medially into the vestibule, the canal is anteroposteriorly elongate (**Figures 12**, **13F**). Despite changes in thickness, the entire course of this canal appears to be arcuate (**Figures 12**, **13**).

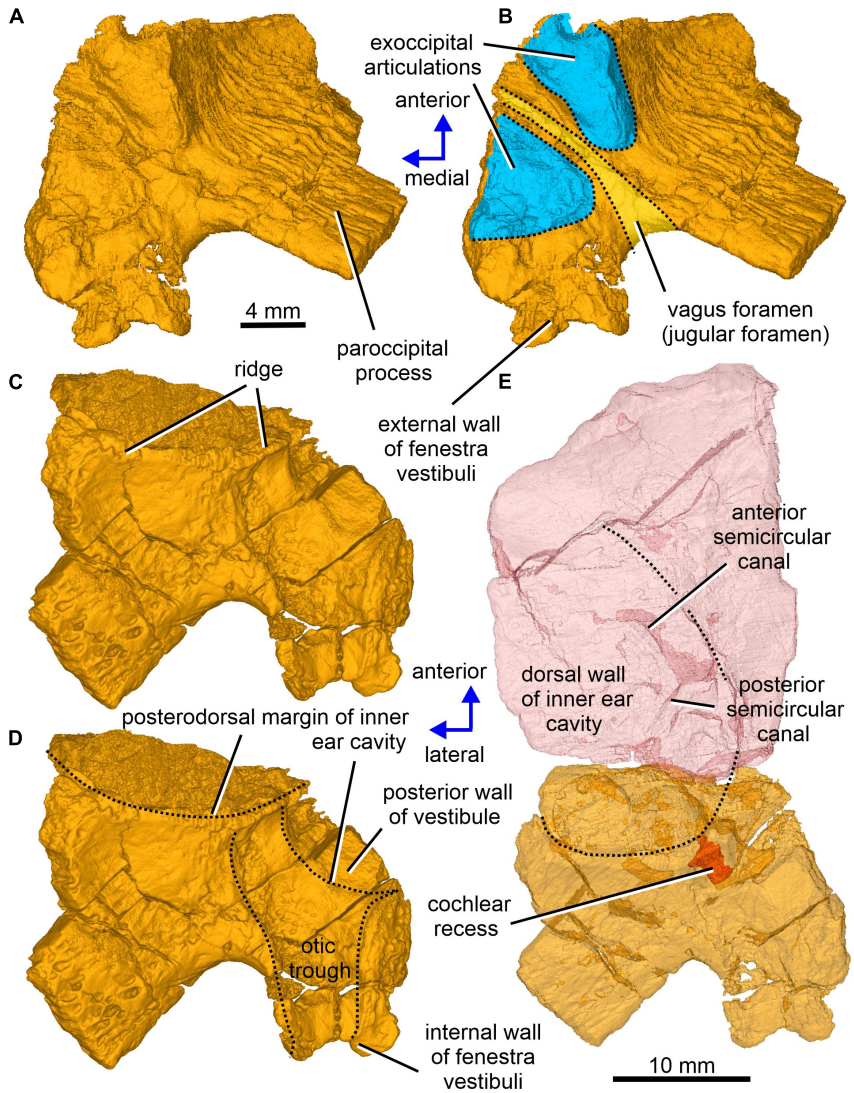

FIGURE 6 | Limnoscelis dynatis, CM 47653. **(A–D)** Right opisthotic in dorsal and slightly anterior view **(A,B)** and ventral and slightly anterior view **(C,D)**. **(E)** Right semitransparent supraoccipital and opisthotic in ventral view.

The posterior semicircular canal is similarly arcuate. Its course can be traced within the supraoccipital and the opisthotic (**Figures 7C**, **12**, **13B,F**). The anterior section of this canal is widest at its junction with the crus commune (**Figures 12**, **13F**). From this point, the canal becomes gradually narrower before merging into a similarly narrow section within the opisthotic (**Figures 7C**, **12**). The posterior extremity of this section enters the vestibule at the same level as the lateral canal (**Figures 7B**, **12**, **13B,F**).

While the anterior and posterior semicircular canals open in part on the cancellous ventral surface of the supraoccipital (**Figures 3C, 4D**), their crus commune opens into the vestibule somewhat ventrally (**Figure 13**), The narrow canal for the endolymphatic duct extends from the posterior wall of the vestibule, immediately anteroventral to the crus commune, and passes into the cranial cavity (**Figures 3B,C, 4B,D, 12, 13A,B,E,F**). The apex of the conical cochlear recess points posteriorly (**Figures 7A, 12, 13B–F**). The recess widens smoothly anteriorly before merging into the vestibule. At this level it becomes mediolaterally narrow and also attains its greatest depth (**Figures 7A,B, 13B–D**).

Phylogenetic Results

We present the results from the unweighted parsimony analysis in the form of strict and Adams consensus topologies (**Figures 14A,B**). The strict consensus reveals loss of resolution across several clades. Eighty-nine per cent of the 165 most parsimonious trees (length = 1285 steps; ensemble consistency index C.I. = 0.2727 without uninformative characters; ensemble retention index R.I. = 0.5814) place diadectomorphs and synapsids as sister taxa. In all trees, the two species of *Limnoscelis*, as sister taxa, join a clade of remaining diadectomorphs,

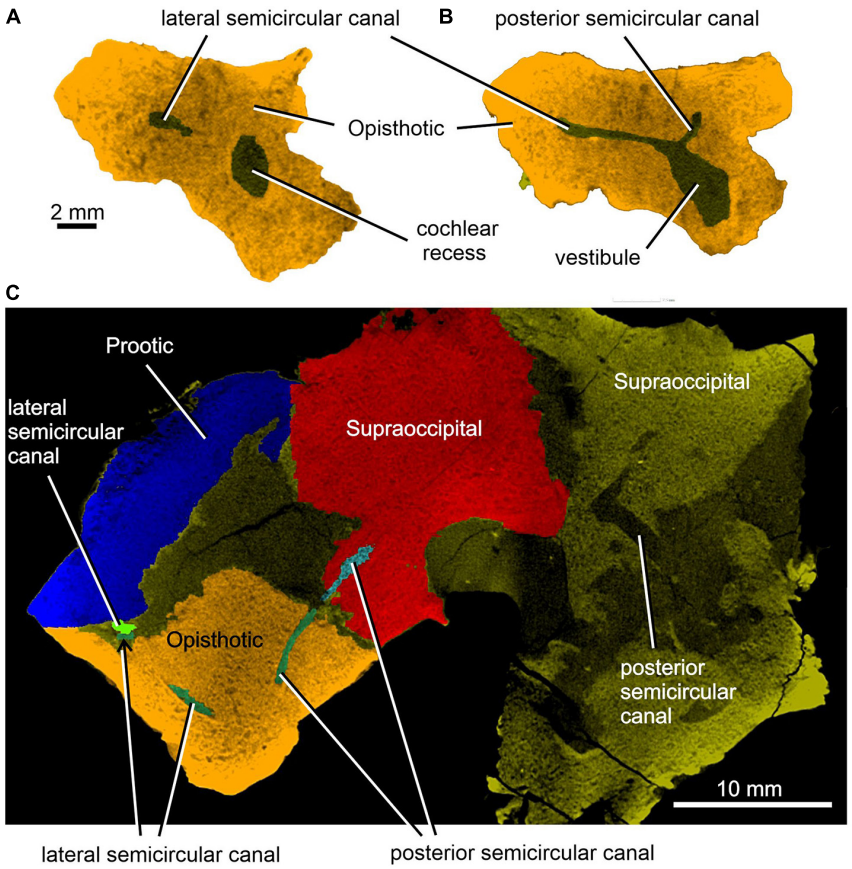

FIGURE 7 | *Limnoscelis dynatis*, CM 47653. **(A,B)** Transverse CT sections through the cochlear recess **(A)** and at the level of the root portions of the lateral and posterior semicircular canals **(B)**. **(C)** Longitudinal CT section through the junction of the opisthotic and supraoccipital portions of the posterior semicircular canals.

which are collapsed in a polytomy. Very few nodes receive high bootstrap and jackknife support and for most, the support is low to moderate, with the majority of nodes in the amniote crown-group collapsed in the bootstrap and jackknife consensus topologies. As noted by Klembara et al. (2020b), although no taxa could be safely deleted (*sensu* Wilkinson, 1996) from the data matrix, the removal of some, especially among anthracosaurs, yields many fewer trees and a more resolved strict consensus topology than the unweighted analysis based upon the full taxon set. For example, when *Eobaphetes kansensis* is deleted, PAUP* produces 12 shortest trees (not illustrated here). In these, a fully resolved clade of diadectomorphs emerges as the sister group to synapsids.

Both the reweighted and the implied weights analysis (**Figures 14C,D**) yield a single tree supporting a diadectomorph-synapsid clade. The reweighted analysis tree has a length of 225,29973 steps with C.I. = 0.4778 without uninformative characters and R.I. = 0.777. The implied weights tree has a length of 1295 steps (Goloboff fit = −201.77756) with C.I. = 0.2705 without uninformative characters and R.I. = 0.5769. In these analyses, the branching pattern of diadectomorphs, synapsids and diapsids is identical, and both retrieve *Westlothiana* and *Solenodonsaurus* as immediate sister taxa to [diapsids + (synapsids + diadectomorphs)]. However, some differences exist in the branching arrangement of stem-group amniotes less crownward than *Solenodonsaurus*. In both, seymouriamorphs form a clade, with *Utegenia* and *Seymouria* as successive sister taxa to remaining species in that clade. In the reweighed analysis, *Karpinskiosaurus* and (*Leptoropha* + *Microphon*) are successive sister taxa to a group that includes (*Ariekanerpeton* + *Discosauriscus*) and (*Makowskia* + *Spinarerpeton*). In the implied weights analysis (*Leptoropha* + *Microphon*) joins (*Ariekanerpeton* + *Discosauriscus*) and this clade joins (*Karpinskiosaurus* + (*Makowskia* + *Spinarerpeton*)). In the reweighted analysis, *Caerorhachis* is the sister taxon to anthracosaurs, with *Calligenethlon* nested within the latter. In the implied weights analysis *Caerorhachis* is nested within anthracosaurs while *Calligenethlon* forms the immediate sister taxon to *Solenodonsaurus* plus more derived groups. Lastly, *Chroniosaurus* is either allied to anthracosaurs (reweighted analysis) or placed as the immediate sister taxon to *Gephyrostegus* plus more derived groups (implied weights analysis).

The Bayesian analysis attained satisfactory convergence, with the average Potential Scale Reduction Factor for the branch

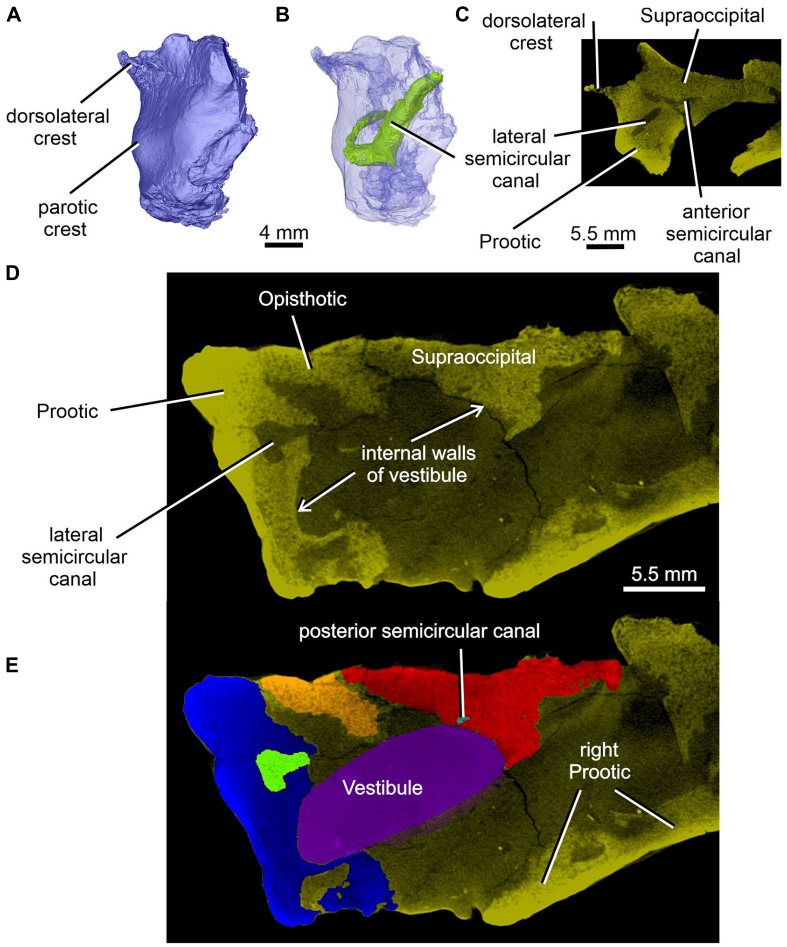

FIGURE 8 | *Limnoscelis dynatis*, CM 47653. **(A,B)** Left prootic in posterolateral view; **(B)** semitransparent. **(C)** Transverse CT section through the left prootic-left supraoccipital in the place of the junction of anterior and lateral semicircular canals. **(D,E)** Transverse CT sections through the walls of vestibule **(D)** and reconstructed vestibule **(E)** at the level of the medial opening of the lateral semicircular canal.

length parameter equal to 1. The Bayesian topology (**Figure 15A**) reveals some differences from that presented in Klembara et al. (2020b). Thus, the colosteid *Greererpeton* emerges as a stem-group tetrapod instead of forming the sister taxon to temnospondyls (*Balanerpeton* plus *Dendrerpeton*), while *Caerorhachis* appears as the most plesiomorphic stem-group amniote plesion instead of forming the immediate outgroup to colosteids plus temnospondyls. Crownward of *Caerorhachis* is a trichotomy including: (1) a clade of *Silvanerpeton* plus *Eldeceeon*; (2) a clade of eoherpetontids (*Eoherpeton*) plus embolomeres (*Proterogyrinus* to *Carbonoherpeton*); (3) a diverse array of groups arranged in crownward sequence as follows: chroniosuchians (*Chroniosaurus*); paraphyletic gephyrostegids (*Gephyrostegus*; *Bruktererpeton*); monophyletic seymouriamorphs (slightly less resolved than in Klembara et al., 2020b); *Solenodonsaurus*; *Westlothiana*; diapsids (*Paleothyris* to *Captorhinus*); synapsids (*Eothyris* to *Varanops*); diadectomorphs. Within diadectomorphs, the two species of *Limnoscelis* join a clade formed by *Tseajaia*, *Orobates* and *Desmatodon-Diadectes-Diasparactus*. In the discussion below, we offer a brief commentary on the results of our phylogenetic analyses, with emphasis on the sister group relationship between diadectomorphs and synapsids.

DISCUSSION

Comparisons With *Limnoscelis paludis*

The other known species of *Limnoscelis*, *L. paludis*, was revised by Berman (2000) and Berman et al. (1992, 2010). The skull length of *L. paludis* specimen YPM 81 (Berman et al., 2010) is about 30 cm, whereas the estimated skull length of *L. dynatis* is about half of that value. In *L. paludis* the supraoccipital, prootic, and opisthotic are fused, and this condition is also seen in other large adult diadectomorphs (Berman, 2000; review in Klembara et al., 2020a). As we have shown, the prootic, opisthotic, and supraocciptal in *L. dynatis* are not fused. For this reason the braincase in specimen CM 47653 of *L. dynatis* may actually belong to either a juvenile or a subadult, a conclusion that appears corroborated by the size of its preserved skull bones matching

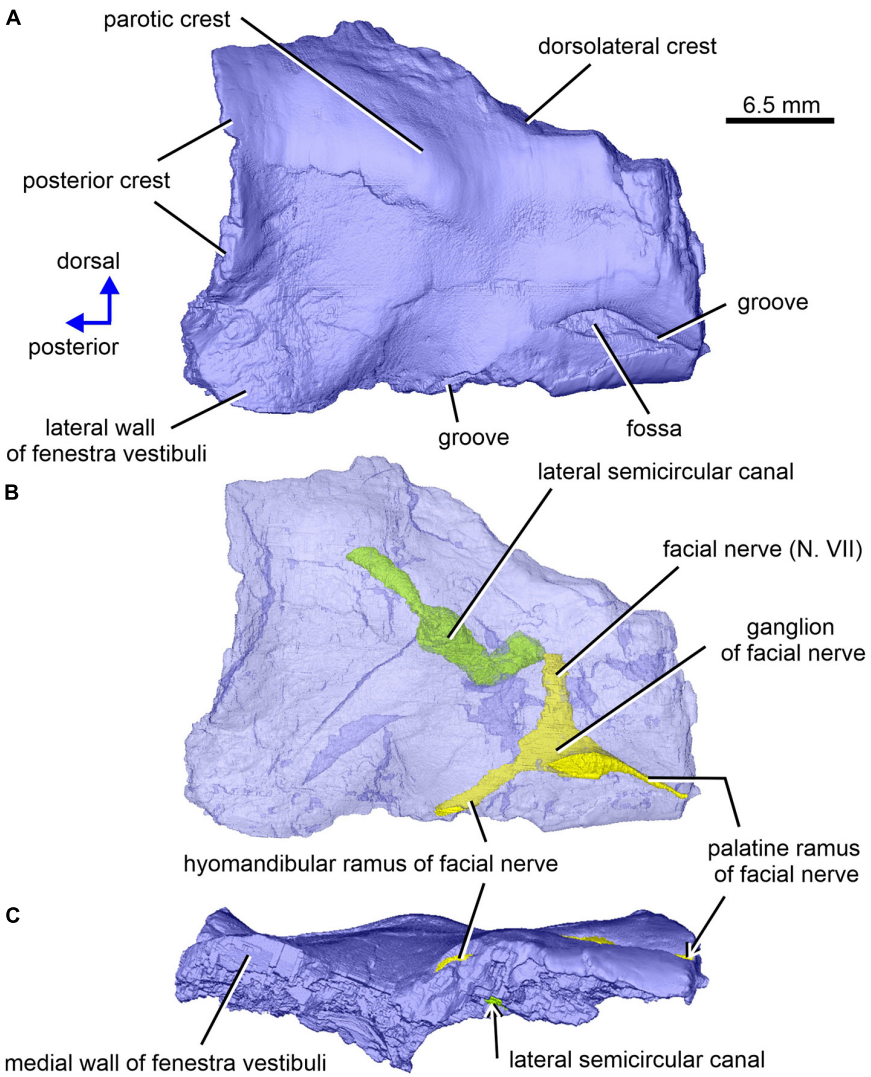

FIGURE 9 | *Limnoscelis dynatis*, CM 47653. Right prootic in lateral and slight posterior **(A,B)** and ventral **(C)** views. **(B)** Semitransparent prootic showing the course of nerves and lateral semicircular canal.

that of juvenile or subadult *D. absitus* (skull length about 12.5 cm; Berman et al., 1998; Klembara et al., 2020b).

In his reconstruction of the *Limnoscelis paludis* braincase, Fracasso (1987) described and reconstructed a synotic tectum as occurring immediately anterior to the supraoccipital. Berman et al. (2010) rejected the presence of this element in both *Limnoscelis* species. Our CT scan data confirm Berman et al.'s interpretation (2010) for *L. dynatis*. Romer (1946) and Fracasso (1987) portrayed the supraoccipital of *L. paludis* as having distinct pointed processes directed laterally and overlapped by conical tabulars (Fracasso, 1987, Figure 2). Such processes are absent in *L. dynatis* (Berman and Sumida, 1990).

In *Limnoscelis paludis* the fused prootic and opisthotic were termed an otic element by Fracasso (1987). In the ventral wall of the posterior half of the otic element, which corresponds to the prootic of *L. dynatis* as described here, Fracasso (1987, Figure 3) identified a deep groove for the vena capitis lateralis and the hyoid ramus of the facial nerve, as well as a distinct parotic crest immediately dorsal to this groove. In *L. dynatis* the parotic crest is well developed, but there is no distinct, dorsally covered groove for the vena capitis lateralis and hyoid ramus of the facial nerve. Instead, the canal for the facial nerve is present in the anterior portion of the prootic that extends dorsomedially to ventrolaterally. The canal bifurcates in the ventral portion of the prootic, giving rise to an anteriorly directed canal. The latter presumably accommodated the palatal ramus of the facial nerve and a posteroventral canal for the hyomandibular branch of the facial nerve in life (**Figure 9**). In this configuration *L. dynatis* closely resembles subadult *Diadectes absitus* (see below). Thus, there appears to be conflicting evidence of the position of the hyomandibular canal in *L. paludis*, such as was presented by Fracasso (1987), and that in *L. dynatis* reconstructed here. In

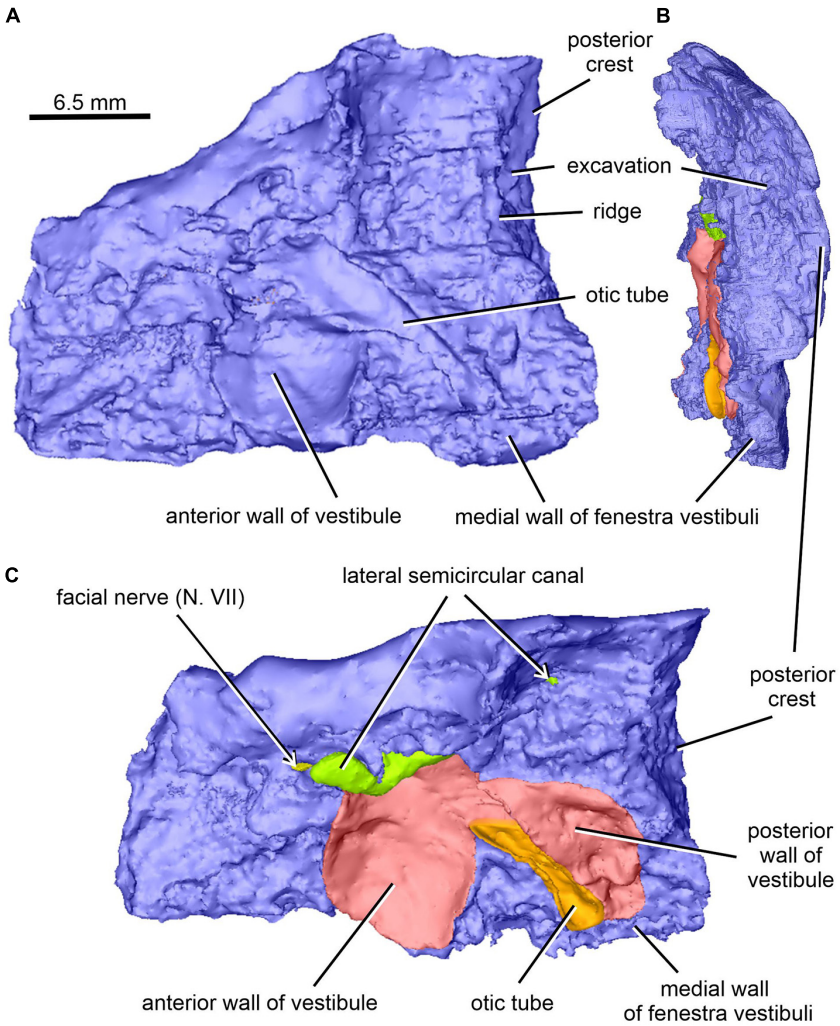

FIGURE 10 | *Limnoscelis dynatis*, CM 47653. **(A–C)** Right prootic in medial **(A)**, posterior **(B)**, and dorsomedial **(C)** views.

light of this, we believe that a novel revision of the braincase of *L. paludis* is required.

Fracasso (1987, Figure 3) described a notch on the anterodorsal portion of the prootic section of his otic element and interpreted it as the exit canal of the trigeminal nerve. A similar smooth-surfaced notch occupies the dorsal margin of the right prootic in *Limnoscelis dynatis*, and this was also interpreted by Berman and Sumida (1990, Figure 4B) as a notch for the trigeminal nerve. The "notch" corresponds in position to a dorsolateral crest on the left prootic. On its right-hand side the crest appears broken and, as a result, the "notch" can be merely attributed to imperfect preservation (**Figures 1A,C**, **9A**). The dorsolateral crest forms the dorsolateral wall of the dorsolateral fenestra. We hypothesize that the trigeminal nerve exit was located much more anteriorly than previously described, presumably along the dorsal margin of the prootic (not preserved). Here, the exit of the trigeminal nerve would lie anterior to the exit of the facial nerve and also anterior to the supraoccipital. A similar configuration is present in the subadult *Diadectes absitus* (Klembara et al., 2020a) and adult *L. paludis* (Fracasso, 1987, Figures 3, 5).

Comparisons With Similarly Sized Diadectids and *Seymouria*

Specimen CM 47653 of *Limnoscelis dynatis* (Berman and Sumida, 1990) is similar in size to the MNG 8747, a subadult specimen of *Diadectes absitus* described by Berman et al. (1998; see also Klembara et al., 2020a,b). In both specimens the neural endocranial bones are not co-ossified, in contrast to the situation observed in the adults of *L. paludis* (Fracasso, 1987; Berman et al., 2010) and certain species of *Diadectes* (for review see Klembara et al., 2020a,b). The skull length of the adult *L. dynatis* is unknown, but the skull length of the adult *L. paludis* is about 30 cm (Berman et al., 2010). The skull length of the subadult *D. absitus* is about 12.5 cm, whereas that of the adult specimens of that species is about 14 cm. The supraoccipital of the subadult *D. absitus* is unpaired, unlike that of *L. dynatis* (see

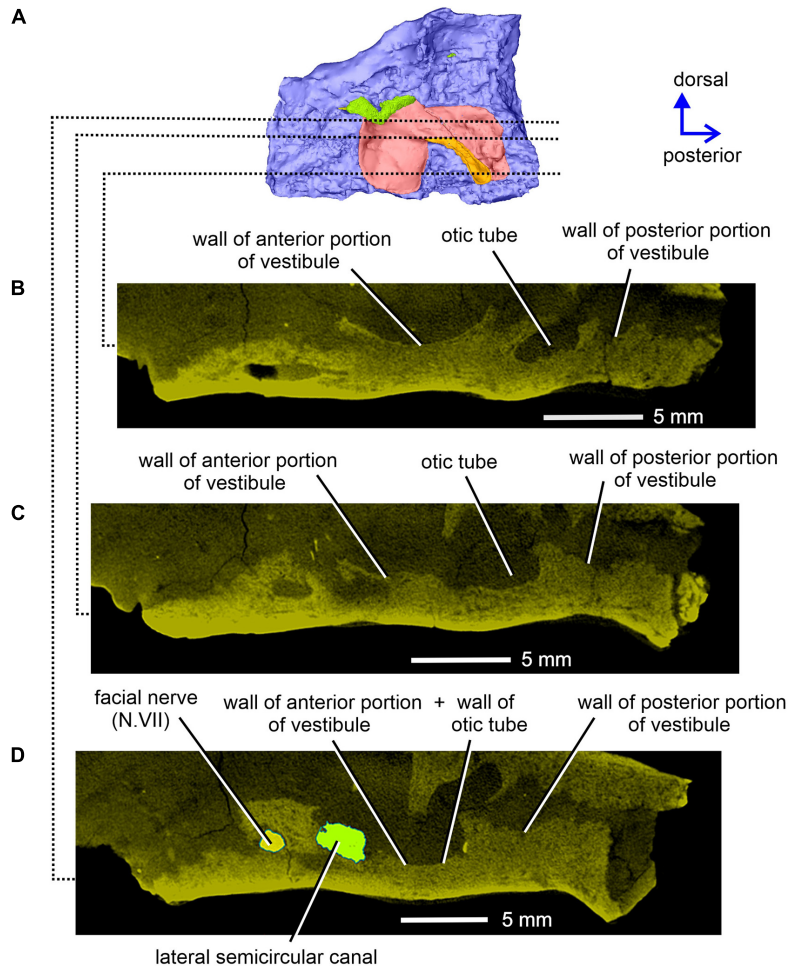

FIGURE 11 | *Limnoscelis dynatis*, CM 47653. Longitudinal CT sections through the right prootic in medial view **(A)** from ventral to dorsal **(B–D)** levels.

also Berman and Sumida, 1990). These observations lend strong support to our interpretation of specimen CM 47653 of *L. dynatis* as belonging to an even earlier ontogenetic stage than specimen MNG 8747 of *D. absitus*. We posit, therefore, that the fusion of the supraoccipital halves in *L. dynatis* must have occurred in comparatively larger skulls than that of *D. absitus*.

Bazzana et al. (2020) described an endochondral ossification situated ventral to the postparietals in *Seymouria*, and interpreted it as the tectum synoticum, but they did not homologize this element with the supraoccipital of crown-group amniotes, despite the topological similarities between the tectum synoticum and the supraoccipital proper. Thus, ontogenetic studies of amniotes demonstrate that the supraoccipital arises from a single ossification center in the tectum synoticum immediately posterior to the parietal (De Beer, 1937; d'A Bellairs and Kamal, 1981). In several birds and mammals the supraoccipital arises from two or more ossification centers in the tectum synoticum (De Beer, 1937). In *Seymouria* the tectum synoticum is located ventral to the postparietals (Bazzana et al., 2020, figure 9). We note that in early crown amniotes the anterior portion of the supraoccipital is covered dorsally by the postparietals and tabulars (Romer, 1976; Romer and Parsons, 1977). In reptiles the postparietal is mostly absent and, as a result, the tectum synoticum is visible in dorsal view. Klembara (2001, figures 2A–C) identified a rudiment of the postparietal, plus the tectum synoticum posterior plus tectum posterius, in late prehatching stages of *Alligator mississippiensis*. The rudiment in question is visible posterior and ventral to the posteriormost margin of the parietal and dorsal to the anteriormost portion of the tectum synoticum posterior plus tectum posterius. Both tecta ossify later in ontogeny to form the supraoccipital. It is likely that the tectum synoticum of *Seymouria* represents an ossified element in the early evolutionary stages of supraoccipital formation. If this is correct, then the tectum synoticum in *Seymouria* should not be identified as the supraoccipital proper, as it is relatively small and is situated below the postparietals only. In contrast, in *Diadectes absitus* and numerous crown amniotes the supraoccipital also underlies the tabulars (Berman et al., 1998; Klembara et al., 2020a). The tectum synoticum of *Seymouria* does not bear the fundamental structures of the supraoccipital that are seen in crown amniotes, such as the medial portions of the anterior and posterior semicircular canals distal to the crus. Perhaps more

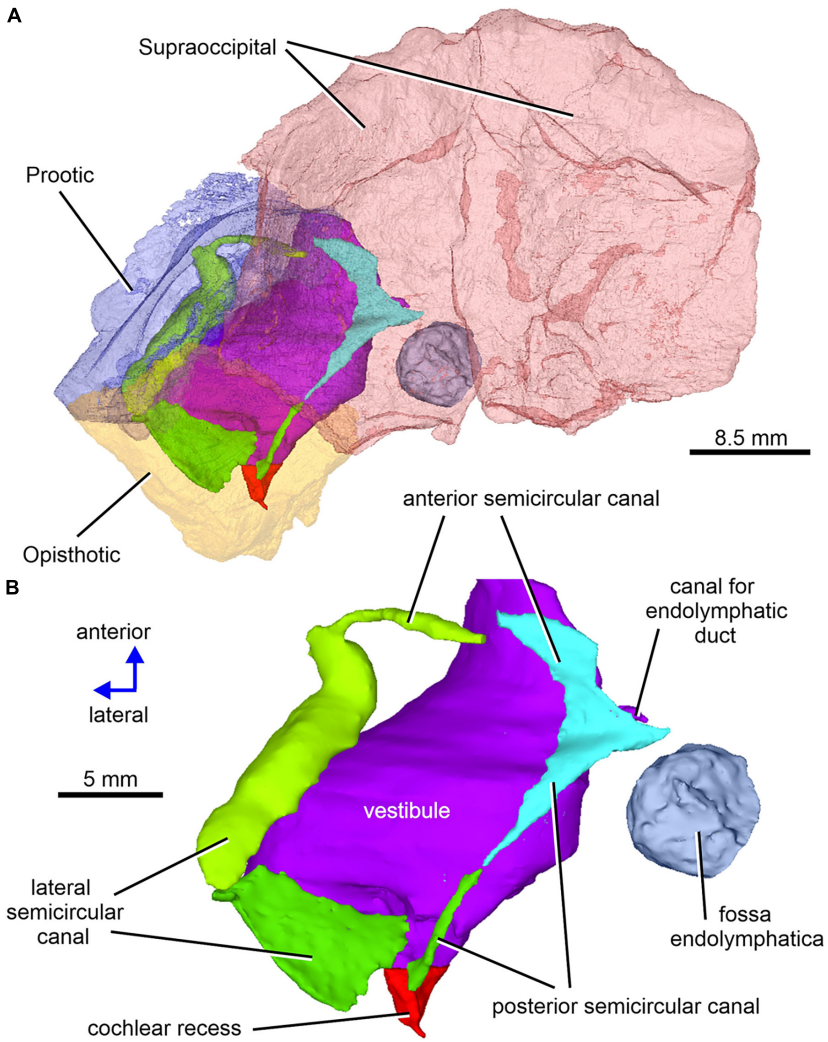

FIGURE 12 | *Limnoscelis dynatis*, CM 47653. **(A)** Left semitransparent prootic, opisthotic and both supraoccipitals to see the position of inner ear structures. **(B)** Virtual 3D model of the inner ear in dorsal view.

significantly, smaller specimens of *Seymouria* show a median suture on the tectum synoticum, a feature that is consistent with a paired origin of the supraoccipital in that genus (Bazzana et al., 2020). This is also the case in *Limnoscelis dynatis* (Berman and Sumida, 1990; see also above).

As for the endocranial elements, the structure described in *Limnoscelis dynatis* as the fossa endolymphatica is absent in *Diadectes absitus* (Klembara et al., 2020a). Among early tetrapods, similar fossae have been recorded only in the stem amniote *Seymouria* and interpreted as the endolymphatic fossae (Bazzana et al., 2020). In *Seymouria* these fossae occur on the ventral wall of the tectum synoticum, which underlies the postparietals. In contrast, in *L. dynatis* the endolymphatic fossae occur on the ventral wall of the posterior portion of the supraoccipitals, and thus further posteriorly relative to the postparietals. The postparietals are not preserved in *L. dynatis*, but their position may be estimated based upon comparisons with their homologues in *L. paludis* (Fracasso, 1987; Berman et al., 2010). In *L. paludis* the unpaired postparietal covers the anterodorsal surface of the supraoccipital. Dempster (1935) described similar fossae in a similar position in the temnospondyl amphibian *Eryops megacephalus*. We note that a supraoccipital is absent in *Eryops* and that the small fossae are present in the prootic of this taxon, at the posterior level of the anterior semicircular canal and slightly anterior to the crus commune. In modern amphibians the size and position of the endolymphatic sac vary in different taxa and the sac occurs at variable distances from the inner ear (Dempster, 1935; Wever, 1985).

In *Limnoscelis dynatis*, the subarcuate fossa is similar in size and position to those in *Diadectes absitus* and *Orobates pabsti*, and occurs anteromedial to the anterior semicircular canal (see Klembara et al., 2020b). In *L. dynatis* all three semicircular canals are arcuate. In contrast, in *D. absitus* the medial portion of the anterior semicircular canal and the entire posterior semicircular

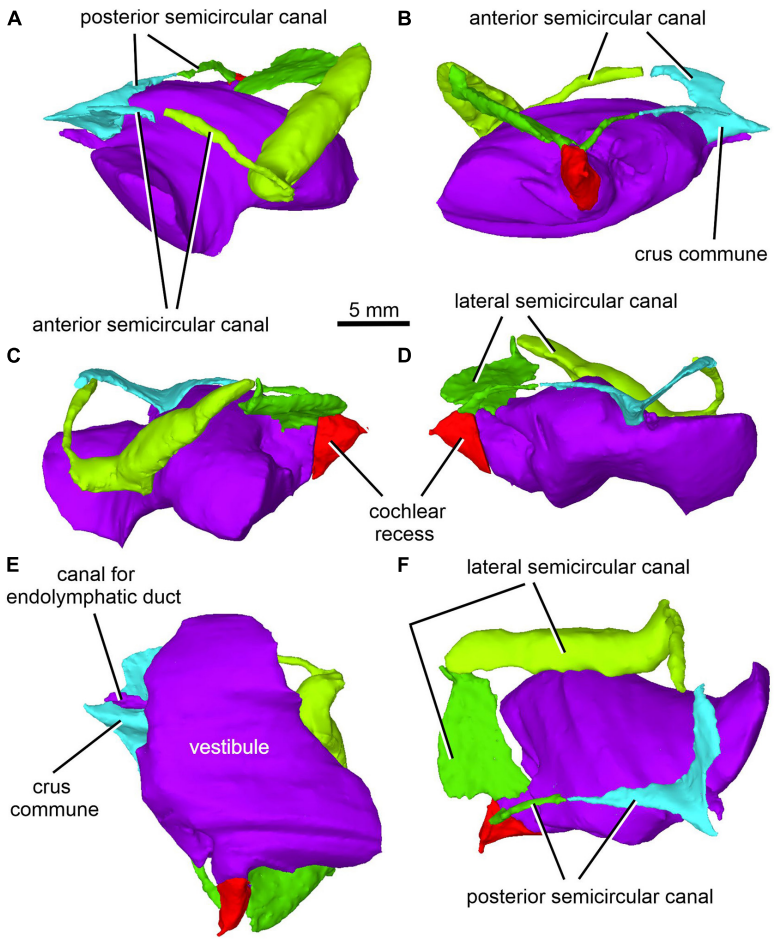

FIGURE 13 | *Limnoscelis dynatis*, CM 47653. Virtual 3D model of inner ear in anterior **(A)**, posterior **(B)**, left lateral **(C)**, right lateral **(D)**, ventral **(E)** and posterodorsal **(F)** views.

canal are straight, and in *O. pabsti* both canals are straight (Klembara et al., 2020b). In all three diadectids, distinct ampullae are absent and the cochlear recess is posterior to the vestibule. The same is true for *Seymouria baylorensis* (Klembara et al., 2020b). Finally, in *D. absitus* and *L. dynatis* the cochlear recess (see also below) is triangular in lateral view (Klembara et al., 2020b).

The lagenar (or cochlear) recess is a variably enlarged cavity excavated within the otic bones of amniotes (Baird, 1970). Neither lissamphibians nor temnospondyls show evidence of this recess (Wever, 1985; Robinson et al., 2005; Sigurdsen, 2008). In extant lissamphibians, the sensory cells associated with hearing (collectively grouped into a lagena, or lagenar macula) are located in the posterior portion of the vestibule (Wever, 1985; Butler and Hodos, 2005; Mason et al., 2015). As first documented in Klembara et al. (2020a), a small but distinct triangular cochlear recess is observed in the stem-group amniote *Seymouria baylorensis* (for a revision of the genus *Seymouria* and a discussion of seymouriamorph morphology and ontogeny, see Klembara, 1997 and Klembara et al., 2006, 2007). In this taxon, the recess occurs within the opisthotic, posterior to the vestibule. A much larger cochlear recess (relative to the size of the vestibule) has also been found in the diadectomorphs *Diadectes absitus*, *Orobates pabsti* (Klembara et al., 2020a,b) and *Limnoscelis dynatis* (as described above). The cochlear recess of *S. baylorensis*, *D. absitus*, *O. pabsti* and *L. dynatis* is situated posterior to the vestibule. Topologically, this position corresponds approximately to that of the lissamphibian lagena, although the latter occurs inside the vestibule. The overall shape of the recess in *D. absitus* and *L. dynatis* matches closely that of several extant amniotes, such as extant lizards (Baird, 1970; Klembara et al., 2020a,b). In modern lizards and in Paleozoic reptiles, such as *Labidosaurus hamatus*, the recess is ventral to the vestibule (Klembara et al., 2020a,b). In *D. absitus* and *O. pabsti* the cochlear recess is partially separated from the vestibule by a vertically orientated slit, but it remains in contact with the vestibule through dorsal and ventral reunient ducts. This partial separation is not observed in *S. baylorensis* and *L. dynatis*.

To summarize the major morphological changes expounded above, and in light of the phylogenetic hypothesis presented here, we posit that early in amniote evolution the cochlear recess arises as a small outpocketing of the posterior wall of the vestibule (endosseous labyrinth) and is in continuity with the latter. This

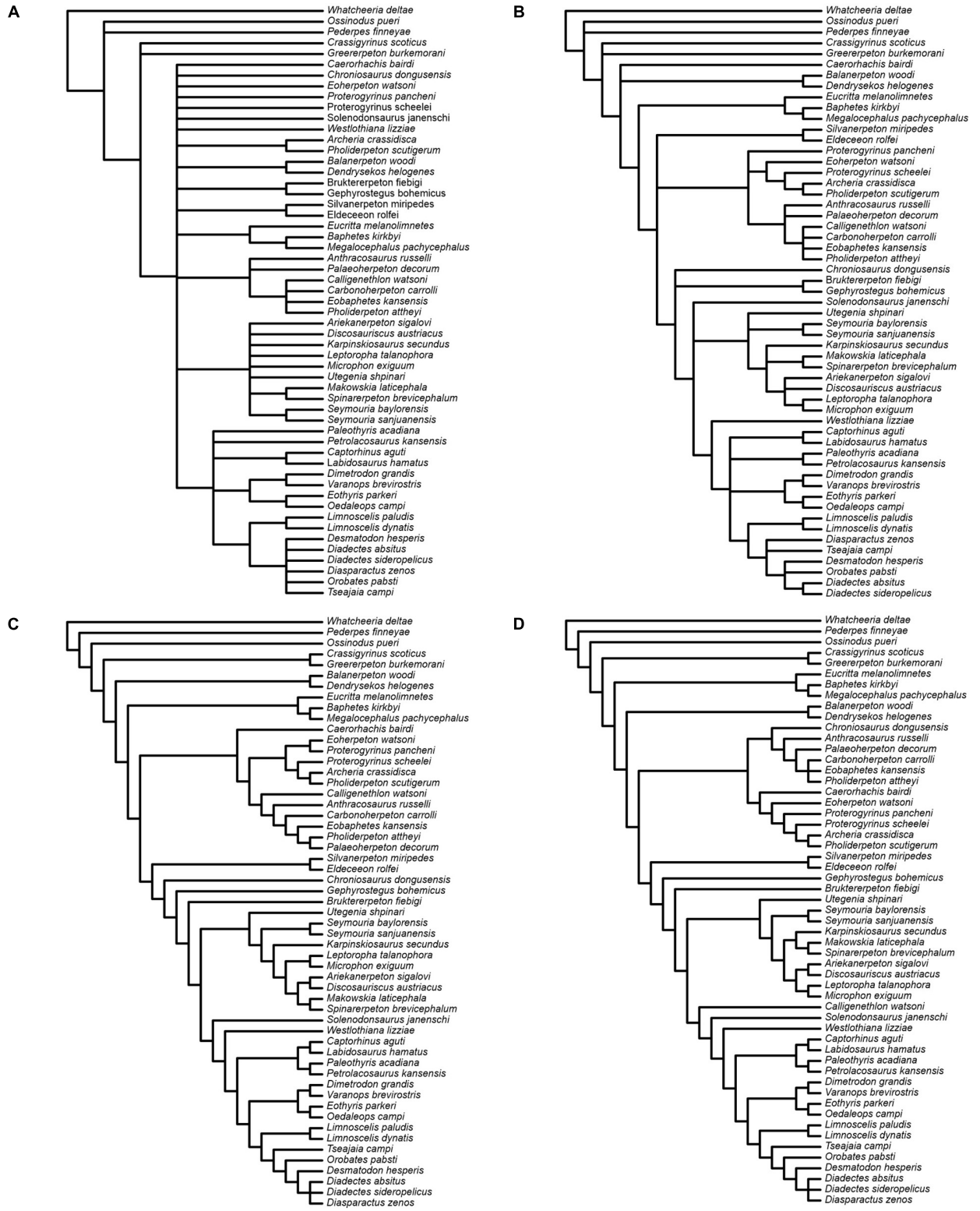

FIGURE 14 | Results of parsimony analyses. **(A,B)** Strict and Adams consensus, respectively, of 165 most parsimonious trees from the analysis with unweighted characters. **(C)** Single tree from the analysis with characters reweighted by the maximum value of their rescaled consistency index from the unweighted analysis. **(D)** Single tree from the analysis with implied weights.

plesiomorphic condition is observed in *Seymouria baylorensis*. As described above, the cochlear recess of *Limnoscelis dynatis* appears to be comparatively larger than that of *S. baylorensis* (a presumably derived condition) but its continuity with the vestibule is maintained (a plesiomorphic condition). In both of these taxa, the cochlear recess is situated posterior to the vestibule, and the latter condition is also seen in *Orobates pabsti* and *Diadectes absitus*. Crucially, the cochlear recess of *O. pabsti* and *D. absitus* is partially separated from the vestibule, its only contact with the latter being established via the reunient ducts. This appears to us as an intermediate stage in the modification of the cochlear recess. Early in amniote evolution, the cochlear recess migrates to a new position, ventral to the vestibule, as exemplified by *Labidosaurus hamatus* and several extant and extinct amniotes (Klembara et al., 2020b).

Bazzana et al. (2020) interpreted certain features visible on the internal surface of the opisthotic in *Seymouria* as inner ear structures. One such feature is the lagenar (cochlear) recess on the ventromedial surface of the medial wall of the opisthotic (Bazzana et al., 2020, Figure 8). Additionally, two depressions situated dorsal to the lagenar recess were interpreted as part of the horizontal semicircular canal, with the posterior semicircular canal lying dorsal to it. Some of these interpretations appear to us to be problematic. As Klembara et al. (2020b) noted, the cochlear recess of *Seymouria baylorensis* is posterior to the vestibule, and a similar spatial relationship occurs in *Limnoscelis dynatis*, *Diadectes absitus,* and *Orobates pabsti*. Klembara et al. (2020b) argued that in amniote evolution, the cochlear recess started to develop as a distinct structure posterior to the vestibule (endosseous cavity). The subsequent step in the evolution of the recess was its anteroventral migration to a new position, ventral to the vestibule (Klembara et al., 2020b). This is the condition shown by *Labidosaurus hamatus* (Klembara et al., 2020b) and *Captorhinus aguti* (Price, 1935; Heaton, 1979). When taken together, these observations suggest that the identity of inner ear structures on the internal wall of the opisthotic in *Seymouria*, such as were noted by Bazzana et al. (2020), may require additional scrutiny.

A final comment concerns the otic tube which extends from the fenestra vestibuli to the vestibule. First described by Watson (1916) in *Diadectes*, the otic tube was later recorded in *Seymouria* (Klembara et al., 2020a,b). As we show here, it is present also in *Limnoscelis dynatis*. Benoit et al. (2017) described a structure called vestibular tube in some synapsids. The structure in question connects the fenestra ovalis to the vestibule and, therefore, it is topologically congruent with the otic tube. Although the function of the tube is unclear, its presence in diadectomorphs and its possible homology with the vestibular tube in synapsids reinforces the possibility that these two groups are closely related (Klembara et al., 2020b).

Comments on Diadectomorph Relationships

The close relationship between synapsids and diadectomorphs is seemingly at odds with current understanding of the taxonomic composition of crown-group amniotes, but perhaps not so unusual. Thus, recent contributions (e.g., Ford and Benson, 2019, 2020) have shown that long-established branching patterns near the roots of the synapsid-sauropsid dichotomy ought to be reassessed (but see also Benoit et al., 2021 for a commentary and a dissenting view), and that homoplasy is widespread. These high levels of homoplasy are not surprising in large-scale data matrices and imply that even subtle permutations of characters may produce substantial branch rearrangements. Despite this, different schemes of character weighting and tree searches under different optimality criteria yield similar patterns of relationships, particularly in the apical portion of the tree. Although we reserve an in-depth treatment of character distribution as part of an ongoing revision of early tetrapod phylogeny, we think it appropriate to comment briefly on the diadectomorph-synapsid clade.

The character-state changes that support this clade are identical in both the reweighted and the implied weights analyses and are also retrieved, albeit with different permutations, in those unweighted topologies in which diadectomorphs and synapsids form sister groups. The following apomorphy list includes character number, character description in bold, consistency index of character (c.i.) and character-state transitions (states are reported in brackets):

1 **nostril morphology**, c.i. = 0.273 (reweighted) or 0.25 (implied weights), round (1) to elliptical and elongate (3);
5 **oblique orientation of anterior surface of premaxilla**, c.i. = 0.333, absence (0) to presence (1);
27 **total length of lacrimal**, c.i. = 0.111 (reweighted) or 0.1 (implied weights), more than (1) to less than (0) two and a quarter times its maximum pre-orbital length;
39 **parietal-postparietal suture**, c.i. = 0.1, strong interdigitation absent (0) to present (1);
40 **lateral parietal lappets**, c.i. = 0.5, absent (0) to present (1);
41 **postparietal occurrence**, c.i. = 0.333, paired (0) to unpaired (1);
88 **dorsal process of quadrate**, c.i. = 0.25, absent (0) to present (1);
90 **nostril size**, c.i. = 0.167, less than (0) to equal to/greater than (1) 50 percent of the size of the choana;
91 **nostril height in lateral projection**, c.i. = 0.1, greater than (0) to equal to/less than (1) the distance between the nostril ventral rim and the upper jaw margin;
101 **pineal foramen diameter**, c.i. = 0.5, less than (0) to more than (1) 33% or greater than the anteroposterior length of the parietal suture;
103 **position of posttemporal fenestra**, c.i. = 1, (1) [fossa present near occiput dorsolateral corner, delimited dorsally by occipital flanges of tabular and postparietal and bordered laterally as well as ventrally by dorsolateral extension of opisthotic meeting tabular ventromedial flange] to (2) [small fossa present near occiput ventrolateral corner, bordered laterally by tabular ventromedial flange, delimited dorsally by dorsal portion of the lateral margin of the supraoccipital–opisthotic complex and floored by lateral extension of opisthotic];

135 **dentition on transverse flange of pterygoid**, c.i. = 0.333, row of large (1) to small (2) teeth;
137 **posterolateral flange of pterygoid**, c.i. = 0.143, absent (0) to present (1);
151 **opisthotic forming a thickened plate fused together with the supraoccipital, preventing the exoccipitals from contacting the skull table**, c.i. = 0.333, absent (0) to present (1);
157 **single median depression on parasphenoid**, c.i. = 0.143, present (1) to absent (0);
169 **dentary fangs generally comparable in size with, or greater than, other dentary teeth, close to symphysial region and usually mesial to marginal dentary teeth**, c.i. = 0.143, absent (1) to present (0);
205 **number of premaxillary teeth**, c.i. = 0.222, four (1) to less than four (2);
208 **cleithrum stem in cross-section**, c.i. = 0.667, single concave face (2) to flattened oval (0);
229 **portion of humeral shaft length proximal to entepicondyle**, c.i. = 0.2, greater (1) to smaller (0) than humerus head width;
237 **posterior iliac process subhorizontal, stout, abbreviated posteriorly and tapering rearward in lateral aspect**, c.i. = 0.333, absent (0) to present (1);
241 **internal trochanter forming a distinct protuberance**, c.i. = 0.125, presence (1) to absence (0);
294 **proportions of posterodorsal margin of pelvis**, c.i. = 1, (3) [gently or poorly pronounced "stepped" profile around ilium-ischium suture, elongate ischium with broadly concave dorsal margin] to (4) [deeply angular dorsal margin of ischium, ischium with stout plate-like shape].

Thus, only two characters (103; 294) are free of homoplasy and only three (40; 101; 208) display low homoplasy (c.i. $\geq$ 0.5). Such high levels of homoplasy are not retrieved solely in the crownward portion of amniote phylogeny and are not unexpected for a similarly sized data matrix. We employ three simple approaches to test whether the data matrix contains phylogenetic information and whether its overall structure, in terms of character-state distributions, differs significantly from random.

Our first approach compares the C.I. obtained from the unweighted parsimony analysis to a theoretical C.I. value extrapolated from simulations, following Klassen et al.'s (1991) approach. The C.I. associated with our data set is 0.2817 (including uninformative characters) and exceeds the minimum theoretical value for a data set with an identical number of taxa (n = 55 taxa in our case). This theoretical C.I., or C.I.$_{random}$, is calculated as $2.937 \cdot n^{-0.9339}$, and represents the threshold value that a real data set "... should exceed to be considered to contain phylogenetic information" (Klassen et al., 1991, p. 446). In the case of 55 taxa, C.I.$_{random}$ = 0.0696. Our second approach compares the observed C.I. to the C.I. that is expected for a matrix of comparable size, based upon Sanderson and Donoghue (1989) linear regressions of C.I. vs. taxon number. The C.I.$_{expected}$, calculated as $0.9 - 0.022 \cdot n + 0.000213 \cdot n^2$, gives a value of 0.3343 for 55 taxa (n = 60 is the recommended maximum number of taxa to which the above formula should be applied). This value is only slightly larger than the observed C.I. Both this and the previous approach allow us to conclude that our data includes a reasonable amount of phylogenetic information. Our third approach compares the length of the most parsimonious trees from the unweighted analysis with a distribution of lengths associated with random trees. The distribution of lengths of 10^7 random trees generated in PAUP* is negatively skewed (g1 statistic = – 0.385049). The length of the shortest tress from the unweighted analysis (1285 steps) is well to the left of the leftmost 5% of this distribution (Hillis and Huelsenbeck, 1992), indicating that the data matrix is non-random.

The six characters that describe inner ear conditions (276–281; see also Klembara et al., 2020b for a discussion) can be mapped on the implied weights and reweighted topologies without homoplasy. Detailed knowledge of the innear ear anatomy in basal synapsids and diapsids is needed before any in-depth evaluation of character polarity can be made. The six characters in question reveal a rather discontinuous distribution as very few taxa (including from among synapsids and diadectomorphs) could be scored. For instance, many inner ear characters were coded as "unknown" in the synapsid and diapsid species included in our data, but we are aware that the inner ear anatomy of more derived taxa from both clades has been documented in great detail (e.g., Benoit et al., 2017). In the following, the distributions of inner ear characters are discussed in relation to the derived state under the accelerated transformation option in PAUP* and with reference to the reweighted or implied weights topologies (**Figures 14C,D**). An enlarged cochlear recess (character 276) emerges as a synapomorphy for all taxa more crownward than seymouriamorphs. The condition of a cochlear recess that is orientated posteroventrally/ventrally relative to the vestibule (character 277) can be scored in only two diapsids in our matrix, but this character has a much wider distribution among crown amniotes (see above). Assuming the correctness of a diadectomorph-synapsid sister group relationship and a plesiomorphic condition for diadectomorphs, this character would be interpreted as a parallel acquisition in the two major clades of crown-group amniotes (e.g., under a delayed transformation optimization in PAUP*). The alternative interpretation implies a reversal in diadectomorphs. The presence of a distinctly developed subarcuate fossa in the braincase bone(s) housing the cerebellar flocculus (character 278) emerges as a synapomorphy for all taxa more crownward than seymouriamorphs. The occurrence of an otic tube (character 279) and an otic trough (character 280) both appear as a reversals (losses) among diapsids, as coded, but we suspect the distribution of this character is much more complicated and polarity decisions are rendered complicated by the absence of virtually any information in taxa less crownward than seymouriamorphs. Finally, the arcuate morphology of the entire or posteromedial section of the anterior semicircular canal and of the entire posterior semicircular canal appears as a reversal in two diadectomorphs, as coded, but again we suspect that polarity decisions ought to be regarded as provisional.

Finally, we tested the influence of inner ear characters on the phylogenetic analysis, following a similar experiment of character deletion in Klembara et al. (2020b). When the six inner ear characters are removed, an unweighted character parsimony

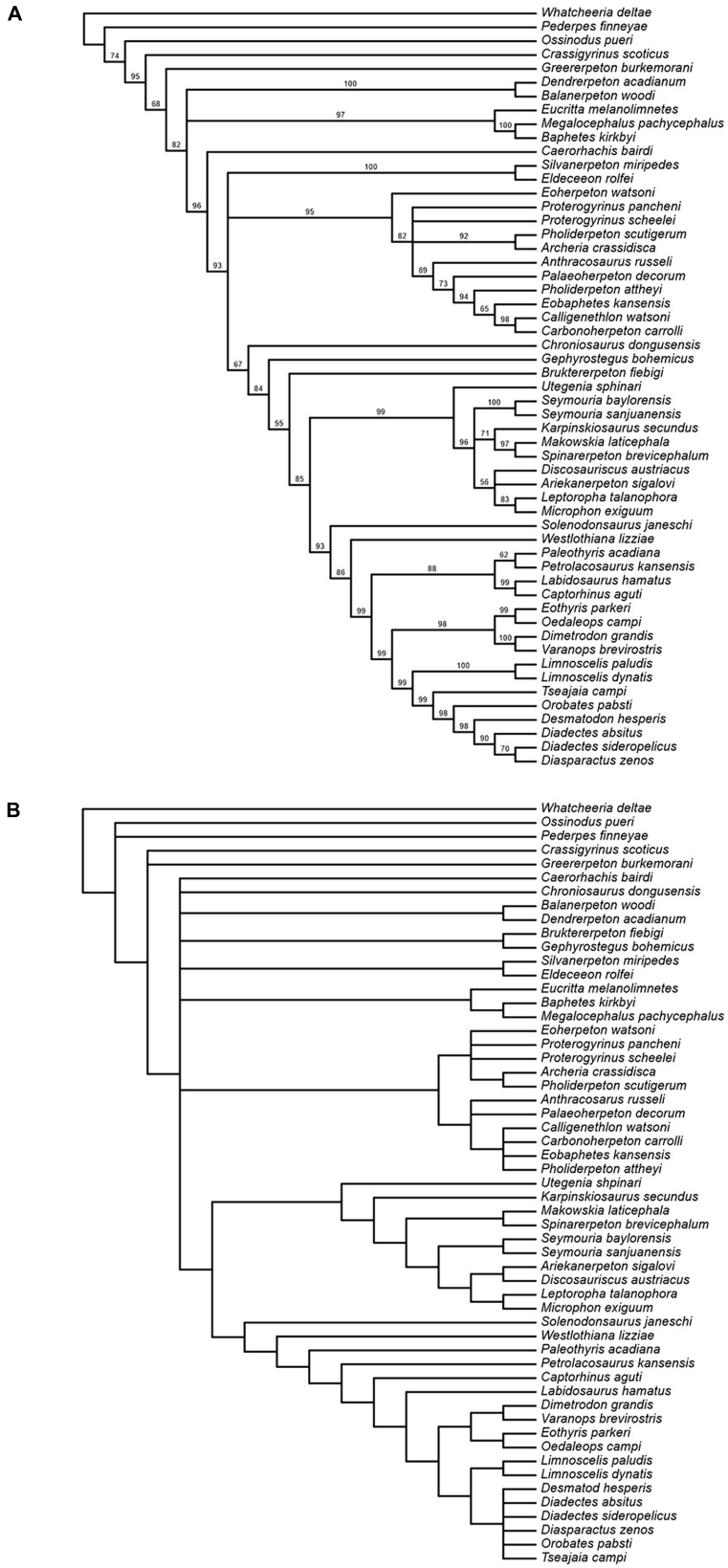

FIGURE 15 | (A) Results of Bayesian analysis; clade credibility tree with posterior probability (credibility) values for node support appended to branches. **(B)** Strict consensus of 78 most parsimonious trees from analysiswith unweighted characters after deletion of inner ear characters.

analysis results in 78 shortest trees (length = 1278 steps; C. I. = 0.2694 without uninformative characters; R.I. = 0.5807), a strict consensus of which is shown in **Figure 15B**. This is slightly more resolved than the strict consensus from the original analysis (**Figure 14A**). In all shortest trees synapsids and diadectomorphs form a clade. Except for the two species of *Limnoscelis*, most diadectomorphs are collapsed in a polytomy, and the analysis fails to provide support for monophyletic diapsids.

CONCLUSION

In conclusion, new data on the braincase and inner ear of *Limnoscelis dynatis* enriches the range of neuroanatomical conditions near the base of crown-group amniotes and expands our knowledge of the anatomy of diadectomorph tetrapods. We hope that the present contribution will encourage additional work on this iconic group and stimulate further discussions on the origin and interrelationships of early amniotes.

DATA AVAILABILITY STATEMENT

The datasets presented in this study can be found in online repositories. The names of the repository/repositories and accession number(s) can be found in the article/**supplementary material**.

AUTHOR CONTRIBUTIONS

JK conceived and designed the project. MH took measurements from CT-scans. MH and JK segmented the CT-scan data. JK, MH, and DB analyzed the CT-scan data. MR performed the phylogenetic analyses. JK and MR wrote the text. JK, MR, and MH assembled the figures. All authors contributed to writing the manuscript, reviewed manuscript drafts, and approved the final version.

FUNDING

This project was supported by the Scientific Grant Agency of Ministry of Education of Slovak Republic and Slovak Academy of Sciences (Grant No. 1/0228/19 to JK) and the Agency of Ministry of Education of Slovak Republic and Slovak Academy of Sciences (Grant/Award No. APVV-14-0719 to MH for CT scans).

ACKNOWLEDGMENTS

We thank Dr. Amy C. Henrici (Carnegie Museum of Natural History, Pittsburgh) for allowing us to examine specimen CM 47653 for this study, Dr. Mark J. MacDougall (Museum für Naturkunde, Leibniz-Institut für Evolutions- und Biodiversitätsforschung, Berlin) for his editorial efforts, and Dr. Julien Benoit (Evolutionary Studies Institute, School of Anatomical Sciences, University of the Witwatersrand, Johannesburg) and Professor Jun Liu (Institute of Vertebrate Paleontology and Paleoanthropology, Chinese Academy of Sciences) for their constructive comments and helpful suggestions, which improved considerably the quality of this work. We are grateful to the Editors of this Research Topic volume for their invitation to contribute our article.

SUPPLEMENTARY MATERIAL

The Supplementary Material for this article can be found online at: https://www.frontiersin.org/articles/10.3389/fevo.2021.709766/full#supplementary-material

REFERENCES

Baird, I. L. (1970). "The anatomy of the reptilian ear." 193–275," in *Biology of the Reptilia, Vol. 2, Morphology B*, ed. C. Gans (New York: Academic Press), 1–374.

Bazzana, K. D., Gee, B. M., Bevitt, J. J., and Reisz, R. R. (2020). Neurocranial anatomy of *Seymouria* from Richards Spur, Oklahoma. *J. Vertebr. Paleontol* 39:e1694535. doi: 10.1080/02724634.2019.1694535

Benoit, J., Kruger, A., Jirah, S., Fernandez, V., and Rubidge, B. S. (2021). Palaeoneurology and palaeobiology of the dinocephalian therapsid *Anteosaurus magnificus*. *Acta Palaeontol. Pol.* 66, 389–393.

Benoit, J., Manger, P. R., Fernandez, V., and Rubidge, B. S. (2017). The bony labyrinth of late Permian Biarmosuchia: palaeobiology and diversity in non-mammalian Therapsida. *Palaeontol. Afr.* 52, 58–77.

Berman, D. S. (2000). Origin and early evolution of the amniote occiput. *J. Paleontol.* 74, 938–956. doi: 10.1666/0022-3360(2000)074<0938:oaeeot>2.0.co;2

Berman, D. S. (2013). "Diadectomorphs, amniotes or not?," in *The Carboniferous-Permian Transition: Bulletin 60*, eds S. G. Lucas, V. A. DiMichele, J. E. Barrick, J. W. Schneider, and J. A. Spielmann (Albuquerque: New Mexico Museum of Natural History and Science), 22–35.

Berman, D. S., Henrici, A. C., Kissel, R. A., Sumida, S. S., and Martens, T. (2004). A new diadectid (Diadectomorpha), Orobatspabsti, from the Early Permian of Central Germany. *Bull. Carnegie Mus. Nat. Hist.* 35, 1–36. doi: 10.2992/0145-9058(2004)35[1:anddop]2.0.co;2

Berman, D. S., Reisz, R. R., and Scott, D. (2010). Redescription of the skull of *Limnoscelis paludis* Williston (Diadectomorpha: Limnoscelidae) from the Pennsylvanian of Cañon del Cobre, Northern New Mexico. *New Mexico Mus. Nat. Hist. Sci. Bull.* 49, 185–210.

Berman, D. S., and Sumida, S. (1990). A new species of *Limnoscelis* (Amphibia, Diadectomorpha) from the Late Pennsylvanian Sangre de Cristo Formation of Central Colorado. *Ann. Carnegie Mus. Nat. Hist.* 59, 303–341.

Berman, D. S., Sumida, S. S., and Lombard, R. E. (1992). Reinterpretation of the temporal and occipital regions in *Diadectes* and the relationships of diadectomorphs. *J. Paleontol.* 66, 481–499. doi: 10.1017/s0022336000034028

Berman, D. S., Sumida, S. S., and Martens, T. (1998). *Diadectes* (Diadectomorpha: Diadectidae) from the early Permian of central Germany, with description of a new species. *Ann. Carnegie Mus. Nat. Hist.* 67, 53–93.

Butler, A. N., and Hodos, W. (2005). *Comparative vertebrate neuroanatomy: Evolution and adaptation, 2nd ed*. Hoboken: John Wiley & Sons.

Case, E. C. (1907). *Revision of the Pelycosauria of North America*. Washington: Carnegie Institution of Washington. 1–176.

Case, E. C. (1914). On the structure of the inner ear in two primitive reptiles. *Biol. Bull.* 27, 213–216. doi: 10.2307/1535976

d'A Bellairs, A., and Kamal, A. M. (1981). "The chondrocranium and the development of the skull in recent reptiles," in *Biology of the Reptilia, Vol. 11,*

Morphology F, ed. C. Gans (New York: Academic Press), 1–263. doi: 10.3724/sp.j.1245.2013.00001

De Beer, G. R. (1937). *Development of the Vertebrate Skull*. London: Oxford University Press.

Dempster, W. T. (1935). The brain case and endocranial cast of *Eryops megacephalus* (Cope). *J. Comp. Neurol.* 62, 171–196. doi: 10.1002/cne.900620108

Farris, J. S., Albert, V. A., Källersjö, M., Lipscomb, D., and Kluge, A. G. (1996). Parsimony jackknifing outperforms neighbour-joining. *Cladistics* 12, 99–124. doi: 10.1111/j.1096-0031.1996.tb00196.x

Felsenstein, J. (1985). Confidence limits on phylogenies: an approach using the bootstrap. *Evolution* 39, 783–791. doi: 10.2307/2408678

Ford, D. P., and Benson, R. B. J. (2019). A redescription of *Orovenator mayorum* (Saurosida, Diapsida) using high resolution mCT, and the consequences for early amniote phylogeny. *Pap. Palaeontol.* 5, 197–239. doi: 10.1002/spp2.1236

Ford, D. P., and Benson, R. B. J. (2020). The phylogeny of early amniotes and the affinities of Parareptilia and Varanopidae. *Nat. Ecol. Evol.* 4, 57–65. doi: 10.1038/s41559-019-1047-3

Fracasso, M. A. (1987). Braincase of *Limnoscelis paludis* Williston. *Postilla* 201, 1–22. doi: 10.1007/978-3-319-23534-9_1

Gelman, A., and Rubin, D. B. (1992). Inference from iterative simulation using multiple sequences. *Stat. Sci.* 7, 457–472. doi: 10.1214/ss/1177011136

Goloboff, P. (1993). Estimating character weighting during tree search. *Cladistics* 9, 83–91. doi: 10.1111/j.1096-0031.1993.tb00209.x

Heaton, M. J. (1979). Cranial anatomy of primitive captorhinid reptiles from the Late Pennsylvanian and Early Permian Oklahoma and Texas. *Bull. Oklahoma Geol. Surv.* 127, 1–84. doi: 10.1130/spe152-p1

Hillis, D. M., and Huelsenbeck, J. P. (1992). Signal, noise, and reliability in molecular phylogenetic analyses. *J. Hered.* 83, 189–195. doi: 10.1093/oxfordjournals.jhered.a111190

Jones, K. E., Angielczyk, K. D., Polly, P. D., Head, J. J., Fernandez, V., Lungmus, J. K., et al. (2018). Fossils reveal the complex evolutionary history of the mammalian regionalized spine. *Science* 361, 1249–1252. doi: 10.1126/science.aar3126

Klassen, G. J., Mooi, R. D., and Locke, A. (1991). Consistency indices and random data. *Syst. Zool.* 40, 446–457. doi: 10.1093/sysbio/40.4.446

Klembara, J. (1997). The cranial anatomy of *Discosauriscus* Kuhn, a seymouriamorph tetrapod from the Lower Permian of the Boskovice Furrow (Czech Republic). *Philos. Trans. R. Soc. Lond. B Biol Sci.* 352, 257–302. doi: 10.1098/rstb.1997.0021

Klembara, J. (2001). The postparietal and prehatching ontogeny of the supraoccipital in *Alligator mississippiensis* (*Archosauria. Crocodylia*). *J. Morphol.* 249, 147–153. doi: 10.1002/jmor.1046

Klembara, J., Berman, D. S., Henrici, A., Čerňanský, A., and Werneburg, R. (2006). Comprison of cranial anatomy and proportions of similarly sized *Seymouria sanjuanensis* and *Discosauriscus austriacus*. *Ann. Carnegie Mus.* 75, 37–49. doi: 10.2992/0097-4463(2006)75[37:cocaap]2.0.co;2

Klembara, J., Berman, D. S., Henrici, A., Čerňanský, A., Werneburg, R., and Martens, T. (2007). First description of skull of Lower Permian *Seymouria sanjuanensis* (Seymouriamorpha: Seymouriidae) at an early juvenile stage. *Ann. Carnegie Mus.* 76, 53–72. doi: 10.2992/0097-4463(2007)76[53:fdosol]2.0.co;2

Klembara, J., Hain, M., Čerňanský, A., Berman, D. S., and Henrici, A. C. (2020a). Anatomy of the neural endocranium, parasphenoid and stapes of *Diadectes absitus* (Diadectomorpha) from the early Permian of Germany based on the high-resolution X-ray microcomputed tomography. *Anat. Rec.* 303, 2951–3170.

Klembara, J., Hain, M., Ruta, M., Berman, D. S., Pierce, S., and Henrici, A. C. (2020b). Inner ear morphology of diadectomorphs and seymouriamorphs (Tetrapoda) uncovered by high-resolution X-ray microcomputed tomography, and the origin of the amniote crown group. *Palaeontology* 63, 131–154. doi: 10.1111/pala.12448

Klembara, J., Ruta, M., Hain, M., and Berman, D. S. (2021). Braincase and inner ear anatomy of the late Carboniferous tetrapod *Limnoscelis dynatis* (Diadectomorpha) revealed by high-resolution X-ray microcomputed tomography. *Front. Ecol. Evol.* doi: 10.3389/fevo.2021.709766

Kuratani, S., Kuraku, S., and Nagashima, H. (2011). Evolutionary developmental perspective for the origin of turtles: the folding theory for the shell based on the developmental nature of the carapacial ridge. *Evol. Dev.* 13, 1–14. doi: 10.1111/j.1525-142X.2010.00451.x

Lewis, G. E., and Vaughn, P. P. (1965). *Early Permian vertebrates from the Cutler Formation of the Placerville area*. Colorado: U. S. Geological. Survey. 1–46.

Liu, J., and Bever, G. S. (2015). The last diadectomorph sheds light on Late Palaeozoic tetrapod biogeography. *Biol. Lett.* 11:20150100. doi: 10.1098/rsbl.2015.0100

Maddin, H. C., Mann, A., and Herbert, B. (2020). Varanopid from the Carboniferous of Nova Scotia reveals evidence of parental care in amniotes. *Nat. Ecol. Evol.* 4, 50–56. doi: 10.1038/s41559-019-1030-z

Mason, M. J., Segenhout, J. M., Cobo-Cuan, A., Quiñones, P. M., and Dijk, P. V. (2015). The Frog Inner Ear: picture Perfect?. *J. Assoc. Res. Otolaryngol.* 16, 171–188. doi: 10.1007/s10162-015-0506-z

Olson, E. C. (1947). The family Diadectidae and its bearing on the classification of reptiles. *Fieldiana Geol.* 11, 1–53. doi: 10.1007/3-540-26571-6_1

Price, L. L. (1935). "Notes on the brain case of *Captorhinus*",in *Proceedings of the Boston Society of Natural History* (Boston :Boston Society of Natural History). 377–385.

Robinson, J., Ahlberg, P. E., and Koentges, G. (2005). The braincase and middle ear region of *Dendrerpeton acadianum* (Tetrapoda: Temnospondyli). *Zool. J. Linn. Soc.* 143, 577–597. doi: 10.1111/j.1096-3642.2005.00156.x

Romer, A. S. (1946). The primitive reptile *Limnoscelis* restudied: *amer. J. Sci.* 244, 149–188. doi: 10.2475/ajs.244.3.149

Romer, A. S. (1976). *Osteology Of The Reptiles*. Chicago: University of Chicago Press.

Romer, A. S., and Parsons, T. S. (1977). *The Vertebrate Body, 5th ed*. Philadelphia: Saunders College Publishing.

Ronquist, F., and Huelsenbeck, J. P. (2003). MRBAYES 3: Bayesian phylogenetic inference under mixed models. *Bioinformatics* 19, 1572–1574. doi: 10.1093/bioinformatics/btg180

Sanderson, M. J., and Donoghue, M. J. (1989). Patterns of variation in levels of homoplasy. *Evolution* 43, 1781–1795. doi: 10.2307/2409392

Schoch, R., and Sues, H.-D. (2019). The origin of the turtle body plan: evidence from fossils and embryos. *Palaeontology* 63, 375–393. doi: 10.1111/pala.12460

Sigurdsen, T. (2008). The otic region of *Doleserpeton* (Temnospondyli) and its implications for the evolutionary origin of frogs. *Zool. J. Linn. Soc.* 154, 738–751. doi: 10.1111/j.1096-3642.2008.00459.x

Swofford, D. L. (1998). *PAUP* Phylogenetic analysis using parsimony (*and other methods). Version 4*. Sunderland, MA: Sinauer Associates.

Watson, D. M. S. (1916). On the structure of the braincase in certain Lower Permian tetrapods. *Bull. Am. Mus. Nat. Hist.* 35, 611–636.

Wever, E. G. (1985). *The Amphibian Ear*. Princeton: Princeton University Press.

Wilkinson, M. (1996). Majority-rule consensus trees and their use in bootstrapping. *Mol. Biol. Evol.* 13, 437–444. doi: 10.1093/oxfordjournals.molbev.a025604

Conflict of Interest: The authors declare that the research was conducted in the absence of any commercial or financial relationships that could be construed as a potential conflict of interest.

Publisher's Note: All claims expressed in this article are solely those of the authors and do not necessarily represent those of their affiliated organizations, or those of the publisher, the editors and the reviewers. Any product that may be evaluated in this article, or claim that may be made by its manufacturer, is not guaranteed or endorsed by the publisher.